UNIVERSITY **POLITEHNICA** OF
BUCHAREST
**Faculty of Applied Chemistry and Materials ScienceDepartment of Bioresources and Polymer Science**

**DOCTORAL SCHOOL OF APPLIED CHEMISTRY AND MATERIALS SCIENCE**

# PhD THESIS SUMMARY

# Advancements in Cellulose Nanomaterials: From Production to Functionalization for Enhanced Composite Materials
# (Thesis Summary)

PhD. candidate: **Faik Bolat**

PhD. supervisor: **Prof. Dr. Ing. Horia IOVU**

**DOCTORAL COMMITTEE**

| | | | |
|---|---|---|---|
| Phd. Supervisor | Prof. Dr. Ing. Horia IOVU | from | University „Politehnica”of Bucharest |
| Member | Prof. Dr. Ing Catalin ZAHARIA | from | University „Politehnica”of Bucharest |
| Member | Conf.Dr. Ing. Celina DAMIA | from | University „Politehnica”of Bucharest |
| Member | Conf.Dr. Ing. Iuliana BIRU | from | University „Politehnica”of Bucharest |
| Member | CS I .Dr. Ing. Verona IORDACHE | from | INCDCP-ICECHIM |

**Bucharest, 2025**

# Contents

Chapter 1 ....4
General Introduction ....4
Originality and Objectives of the PhD Thesis....5
CHAPTER 2 ....6
2.1. Objectives of the research study ....6
2.10. Results ....7
2.10.1. Hydrodynamic Characteristics and Zeta Potential of the Investigated CNC Samples....7
2.10.2. FTIR Analysis ....9
2.10.3. Raman Spectroscopy....10
2.10.4. XRD....11
2.10.5. Scanning Electron Microscopy (SEM)....12
2.10.6. TG Analysis....14
2.11. Conclusions of the 1st study....16
CHAPTER 3 ....16
**CNC Modification with Acrylic acid and Furfuryl Amine Through Diels-Alder and Michael Addition Reactions**....16
3.1. Objectives of the research study ....16
3.1.2. Chemical modification of CNC with Acrylic acid (CNC-AA) and Reaction of CNC-AA with Furfuryl amine ....16
3.7. Results and discussion ....18
3.7.3. Fourier Transformed Infrared Spectrometry (FT-IR) ....18
3.7.4. X-ray Photoelectron Spectroscopy (XPS) ....19
3.7.5. Thermogravimetric analysis (TGA) ....21
3.7.6. Differential Scanning Calorimetry (DSC)....22
3.7.7. Scanning Electron Microscopy (SEM) ....23
3.8. Conclusions of the 2nd Study :....24
CHAPTER 4 ....24
4.1. Objectives of the research study ....24
4.6.1. Grafting of MDI onto the CN surface ....25
4.6.2. Grafting of NCO-terminated CN-MDI with castor oil....25
4.6.3. PLA-CNC-Based Nanocomposite Synthesis ....26
4.8. Results and Discussion....27
4.8.1. FTIR Analysis of CNC and Modified CNC Samples....27

4.8.2. XPS Analysis of CNC and modified CNC samples ..... 28
4.8.3. DSC Analysis of CNC and modified CNC samples ..... 30
4.8.4. TG Analysis of CNC and modified CNC samples ..... 31
4.8.5. Contact Angle (CA) Analysis of CNC and modified CNC samples ..... 32
4.8.6. SEM Analysis of CNC and modified CNC samples ..... 33
4.8.7. FTIR Analysis of CNC- PLA Nanocomposites ..... 34
4.8.8. DSC Analysis of CNC-PLA Nanocomposites ..... 35
4.8.9. TG Analysis of CNC-PLA Nanocomposites ..... 36
4.8.10. Mechanical Tests of PLA-CNC Nanocomposites ..... 38
4.8.12. SEM Analysis of PLA-CNC Nanocomposites ..... 40
4.9. Conclusions ..... 41
GENERAL CONCLUSIONS ..... 41
SELECTIVE REFERENCES ..... 42
Scientific Publications ..... 43

# *Acknowledgments*

I'm deeply thankful to the members of my committee, Prof. PhD Eng. Cătălin ZAHARIA, Assoc. Prof. PhD Eng. Celina-Maria DAMIAN, Assist. Prof. PhD Eng. Elena Iuliana BÎRU for accepting to review my PhD work. Special thanks to Prof. Dr. Horia IOVU for being as jury president. I appreciate all the helpful feedback and discussions about my manuscript and defense.

I would like to thank my thesis supervisor, Prof. Dr. Horia IOVU, for his patience, support, and guidance throughout my doctoral studies. His observations, advice, and immense enthusiasm give me a good impression. I also would like to thank Dr. Elena Iuliana BIRU, Dr. Jana GHITMAN, Dr. Eugeniu Vasile, and Dr. Anamaria ZAHARIA for their constant help with experiments and analyses of results.

I would like to thank especially my colleague Madalina Ioana NECOLAU who supported and helped me with experiments and analyses of results, without her contribution I couldn't have accomplished the thesis.

I also wish to thank my friend and colleague Kadir Duman for always been there, giving me his support and advice.

My sincere gratitude also goes to all my colleagues and friends in the Materials and Chemistry departments for helping me inside and outside the lab.I would like to thank Polytechnic University in Bucharest for supplying the raw materials and chemicals for my experiments.

# Chapter 1

# General Introduction

Cellulose nanomaterials have emerged as the most promising materials in modern research due to the growing demand for sustainable and high-performance materials. CNMs include cellulose nanocrystals (CNCs) and cellulose nanofibrils (CNFs) produced from renewable resources such as plant fibers and agricultural residues. Cotton is a promising feedstock for extracting nanocellulose materials because of its high purity and abundance. Pretreatment procedures, such as bleaching cotton fibers with hydrogen peroxide ($H_2O_2$) or sodium hypochlorite (NaClO), are usually carried out to remove lignin and hemicellulose, thus increasing the purity and crystallinity of the cellulose. In this respect, nanomaterials with outstanding mechanical strength, thermal stability, and high surface area may be produced by combining different chemical, enzymatic, and mechanical hydrolysis methods accordingly. [C-1, 4,9,13]. Although much importance is given to the extraction techniques in obtaining high-quality nanocellulose, its subsequent functionalization is the only way to realize its full potential for advanced applications.

The hydrophilic nature of nanocellulose hinders perfect integration with nonpolar polymer matrices, which usually produces poor dispersion and hence low performances in hydrophobic systems. Surface functionalization of CNCs has thus been recognized as a very significant approach toward better compatibility, superior interfacial adhesion, and tailoring properties to satisfy the needs of a certain application. Functionalized CNCs hold great promise for biodegradable composites, lightweight material applications, and advanced packaging solutions due to their resultant properties in mechanical and thermal performances [C3/10,11]. The present research aims to advance CNC functionalities for next-generation material creation with specific tailored properties. Following this goal, one innovative grafting strategy will involve the chemical modification of the surface of CNC with acrylic acid through a Diels-Alder/Michael addition reaction using furfuryl amine. The introduced targeted chemical groups through such reactions improve the dispersibility of CNCs in hydrophobic matrices, like PLA, and result in a generally improved performance of such composites. This technique will not only provide sustainable routes for modifying nanocellulose but also reduce the environmental impact resulting from conventional chemical treatment of this biomaterial [C-3/14,15].

The work builds on the functionalization of CNCs by investigating their incorporation into PLA-based composites using both solvent casting and Pickering emulsion methods. These methods are pursued to achieve proper dispersion and strong interfacial bonding, where Pickering emulsion significantly enhances the tensile strength, crystallinity, and overall performance of such materials. These biodegradable composites offer an environmentally friendly alternative for packaging applications, among others, which rely on mechanical strength, along with environmental concerns [C-4/36,53,74]. The structure of this dissertation reflects the comprehensive approach taken to advance the field of nanocellulose. Chapter 1 provides a detailed review of the literature, outlining the challenges and opportunities in nanocellulose production, functionalization, and applications. Chapter 2 discusses the extraction of CNCs from cotton using optimized hydrolysis methods, providing the foundation for surface modification.

Chapter 3 describes the pathways of chemical functionalization, by grafting acrylic acid followed by the reaction of furfuryl amine in Diels-Alder and Michael addition reactions. Chapter 4 assesses the fabrication and performance of PLA composites reinforced with CNC, comparing different processing techniques to find the most effective approaches. Finally, Chapter 5 summarizes the findings and highlights future directions for scaling up these innovations for industrial use. The present work will fill the gaps in sustainable material design through functionalization and application of nanocellulose, thus paving the way for renewable resources toward advanced composite technologies. The insights presented here go beyond the understanding of surface modification techniques to open new possibilities for creating high-performance, eco-friendly materials tailored to meet diverse industrial needs.

# Originality and Objectives of the PhD Thesis

This doctoral dissertation represents a new and wide-reaching research into the functionalization of CNCs and their inclusion into biodegradable polymer composite materials. The originality of the work presented in this thesis is embedded in the following aspects:

- **Sustainable Pretreatment Methods**

This research compares conventional bleaching methods (using hydrogen peroxide, $H_2O_2$) with more environmentally friendly alternatives (such as sodium hypochlorite, NaClO) to assess how these methods influence the quality and properties of extracted cellulose nanocrystals (CNCs). Emphasis is also placed on enzymatic hydrolysis as a greener alternative, highlighting the sustainable approach adopted in this study. Additionally, a combined system of chemical, enzymatic, and mechanical routes is explored to enhance the extraction of CNCs from cotton fibers.

- **Innovative Functionalization Techniques**

Novel chemical reactions were employed for surface modification of CNCs, including acrylic acid grafting followed by Diels-Alder and Michael addition reactions using furfuryl amine. These methods introduce targeted functional groups that improve CNC compatibility with hydrophobic polymer matrices, such as polylactic acid (PLA), while maintaining environmental sustainability. The functionalized CNCs were characterized for chemical, thermal, and morphological changes, providing insights into the effectiveness of the modification.

- **Advanced Composite Fabrication**

This research investigates two techniques for incorporating functionalized CNCs into PLA composites: **solvent casting** and **Pickering emulsion**. The goal is to improve dispersion and interfacial bonding, ultimately enhancing the mechanical and thermal properties of the resulting composites. These methods provide critical insights into achieving superior composite materials with enhanced eco-friendly properties.

- **Application-Oriented Innovation**

The study addresses the challenge of integrating hydrophilic CNCs into nonpolar polymer systems and proposes scalable, industrially relevant solutions, particularly for biodegradable packaging and high-performance materials. By combining advanced functionalization strategies with principles of green chemistry and application-focused methodologies, this work pushes the boundaries of nanocellulose research.

The primary objective of this PhD thesis is to design functionalized CNCs and integrate them into polymer composites to create high-performance, sustainable materials. The research evaluates the **mechanical, thermal, and crystallinity** properties of the CNC-PLA composites concerning the functionalization and fabrication methods used. The study also explores the **environmental viability** of these materials, particularly for **biodegradable packaging** applications.

# CHAPTER 2

A Comparative Study of the Impact of the Bleaching Method on the Production and Characterization of Cotton-Origin Nanocrystalline Cellulose by Acid and Enzymatic Hydrolysis

## 2.1. Objectives of the research study

The main objective of this study is the extraction of nanocellulose materials (cellulose nanocrystals or nano-fibrils) from commercial cotton using two distinct bleaching processes ($H_2O_2$ and NaOCl) with alkali (4 wt.% NaOH), followed by acid ($H_2SO_4$ and HCl) treatment and enzymatic hydrolysis. The novel aspect of this research is comparing the traditionally used NaOCl bleaching method with the more environmentally friendly H2O2 pretreatment method to understand how different types of pretreatments and bleaching methods affect the physical and mechanical properties of extracted CNC or CNF with potential commercial applications.

**Pretreatment of Cotton Fibers:**

- **Cleaning:** Cotton fibers were cleaned with distilled water (1:10 ratio of cotton to water) and dried at 50°C for 24 hours.
- **Delignification:** The fibers were treated with a 2:1 mixture of toluene and ethanol for 24 hours to remove lignin.
- **Impurity Removal:** Samples were washed with 95 wt.% ethanol, then heated at 80°C for 3 hours.
- **Bleaching Methods:**
    - **Method 1:** Fibers bleached with 20 wt.% $H_2O_2$ and 4 wt.% NaOH at 80°C for 4 hours.
    - **Method 2:** Fibers bleached with 16 wt.% NaOCl and 4 wt.% NaOH at 80°C for 4 hours.

**2. Extraction of Nanocellulose Particles:**

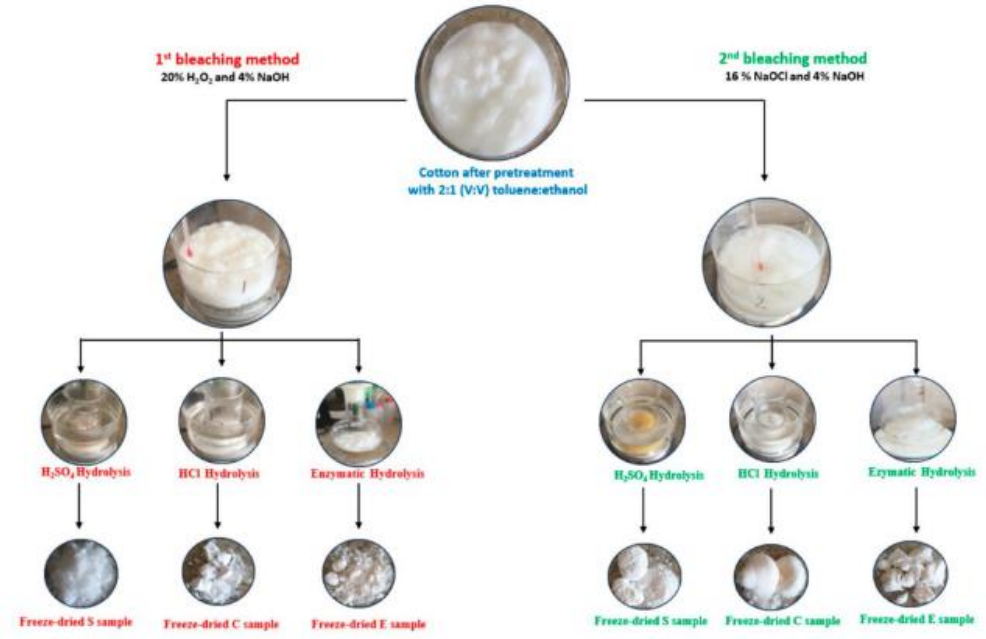
**Acid Hydrolysis Methods:**

1. **$H_2SO_4$ Hydrolysis:**
    - Pretreated cotton (2 g) was mixed with 60 wt.%, 50 wt.%, or 40 wt.% $H_2SO_4$ solutions (1:50 ratio) and stirred for varying durations (10, 20, and 30 minutes) at 70°C.
    - Hydrolysis was stopped by diluting 1 L of deionized water.
    - Six samples were collected based on bleaching method and hydrolysis conditions.
2. **HCl Hydrolysis:**
    - Pretreated cotton (2 g) was treated with 10 wt.%, 15 wt.%, or 20 wt.% HCl solutions and stirred for 20, 40, or 60 minutes at 75°C.
    - Process followed the same steps as $H_2SO_4$ hydrolysis, resulting in six samples.

- **Neutralization:** After the acid hydrolysis, the residue was neutralized with 5% ammonia or 10% acetic acid, washed until neutral pH, centrifuged, and freeze-dried. The final CNC exhibited a flake-like structure with some fibrillar particles.

**Enzymatic Hydrolysis Method:**

- **Setup:** 1 g of pretreated fibers were suspended in 100 mL sodium citrate buffer (pH 4.0), and stirred at 50°C for 30 minutes.
- **Enzyme Treatment:** Mixtures of xylanase (290,000 U/g) and cellulase (500,000 U/g) were added in varying amounts and incubated at 50°C for 24 hours.
- **Termination:** The reaction was stopped by heating at 96°C for 15 minutes.
- **Sample Variations:** Six samples were collected based on enzyme concentration and pretreatment method.




## 2.10. Results

### 2.10.1. Hydrodynamic Characteristics and Zeta Potential of the Investigated CNC Samples

The stability of the CNC dispersion is determined by the Zeta potential or the potential difference at the shear plane of colloidal particles. A high Zeta potential value, above ±30 mV, reflects good stability via electrostatic repulsion, whereas a low value leads to particle aggregation. Sulfuric acid hydrolysis gave the highest stability, ranging from a zeta potential of −42 mV to −32.8 mV, attributed to sulfate groups. In contrast, HCl hydrolysis resulted in lower stability, ranging from −20.2 to −20.3 mV, due to fewer surface charges. Enzymatic hydrolysis showed moderate stability, ranging from −26.4 to −25.4 mV, enhanced by citrate ions.

**Table 4.** The stability of colloids is based on the zeta potential value .

| Zeta Potential (mV) | Stability Behavior |
|---|---|
| 0 to ±5 | Rapid coagulation |
| ±10 to ±30 | Incipient instability |
| ±30 to ±40 | Moderate stability |
| ±40 to ±60 | Good stability |
| >61 | Excellent stability |

Particle sizes in this work ranged from 77 nm ($H_2SO_4$ hydrolysis) to 539 nm, and smaller particles were associated with increased acid concentration and effective bleaching methods. The samples hydrolyzed by sulfuric acid (1S1 and 2S1) developed stable, homogeneous suspensions during the over 72-hour test, whereas sedimentation occurred for all samples subjected to enzymatic hydrolysis because of a larger particle size and consequently lower zeta potential. These results underline the major effects of hydrolysis methods and zeta potential on CNC dispersion stability and particle size.

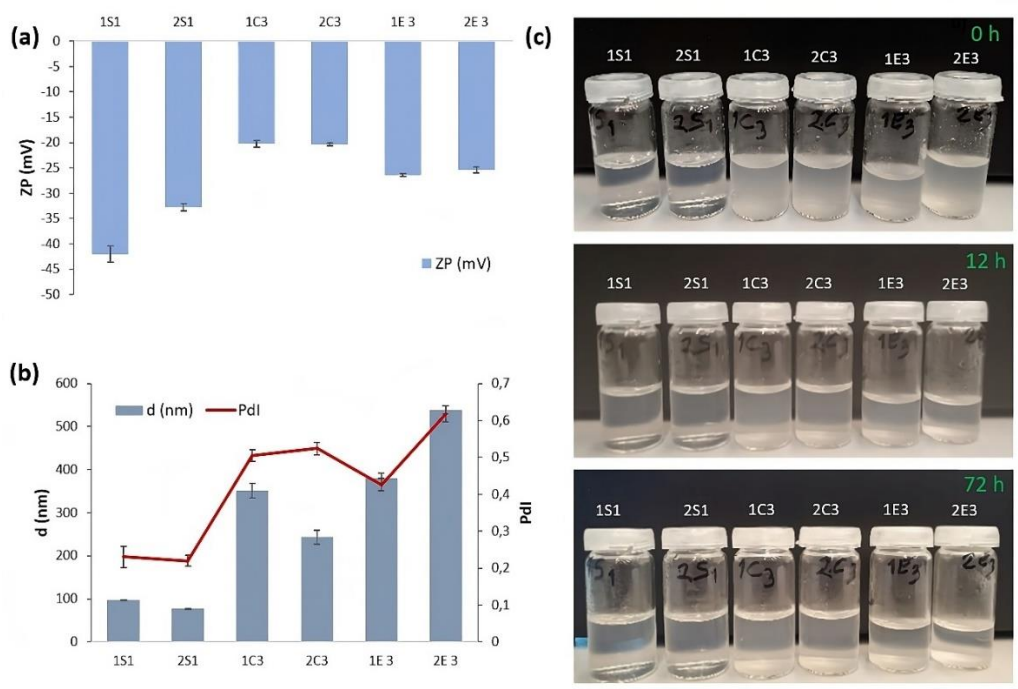



**Figure 2.6.** (**a**) Zeta potential for extracted CNCs in a 0.1 wt.% dispersion; (**b**) mean diameter and PdI and (**c**) photographs of apparent stability of all the investigated samples after 72 h.

## 2.10.2. FTIR Analysis

FTIR was used to examine the chemical structure of the synthesized CNC samples and raw cotton, and the corresponding spectra are presented in Figure 2.7

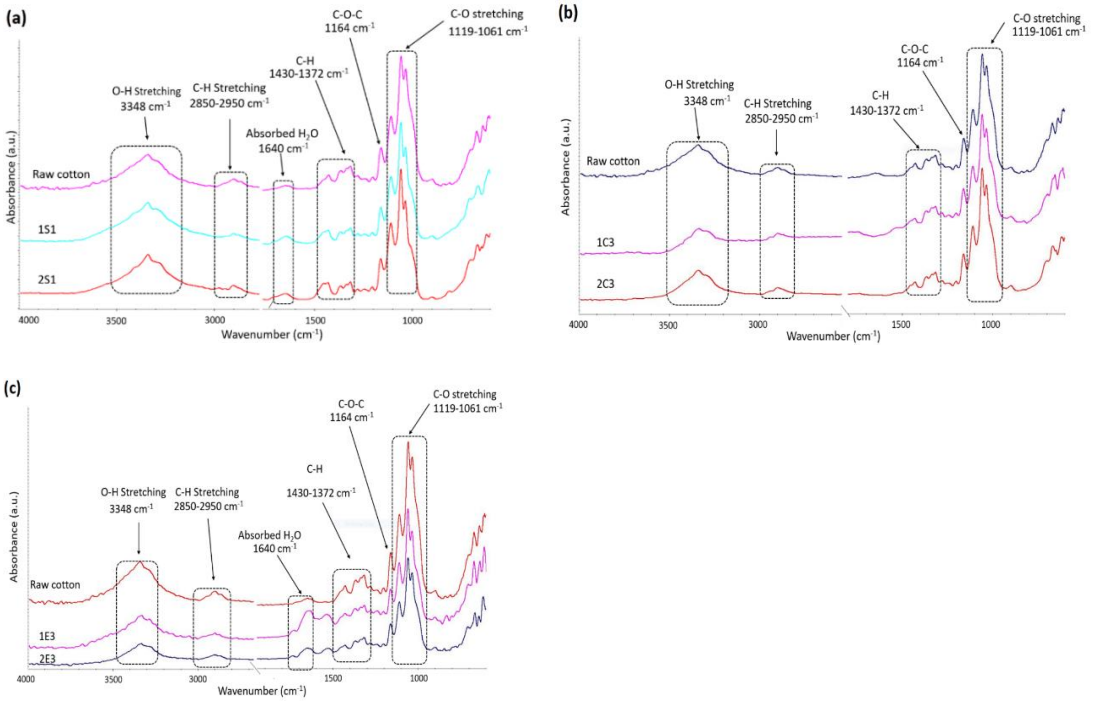



Figure 2.7. FTIR spectra of CNC samples obtained through (**a**) $H_2SO_4$ hydrolysis; (**b**) HCl and (**c**) enzymatic hydrolysis along with raw cotton.

Absorption peaks of CNC samples could be observed in the FTIR spectra with characteristics for cellulose structure. The broad peaks at 3400-3300 cm-¹ correspond to the vibrations of the OH group, corresponding to the crystalline cellulose band. Absorption peaks at 2900-2800 cm-¹ are due to CH stretching. A peak at 1400 cm-¹ is assigned to $CH_2$ bending vibration. Further peaks were observed at 1164 cm-¹ (stretching of C-O-C glycosidic) and 1119-1061 cm-¹ (stretching of bond C-O).

Structural differences are observed among the samples. Sulfuric acid and enzymatic hydrolysis samples have a peak at 1640 $cm^{-1}$, which is assigned to adsorbed water, while HCl hydrolysis and raw cotton samples do not have this peak, indicating efficient removal of water in these samples. The absence of peaks at 1726 $cm^{-1}$ (C=O) and 1550–1533 $cm^{-1}$ (carboxylate doublet) confirms the removal of hemicellulose and lignin, indicating high cellulose purity across all samples.

## 2.10.3. Raman Spectroscopy

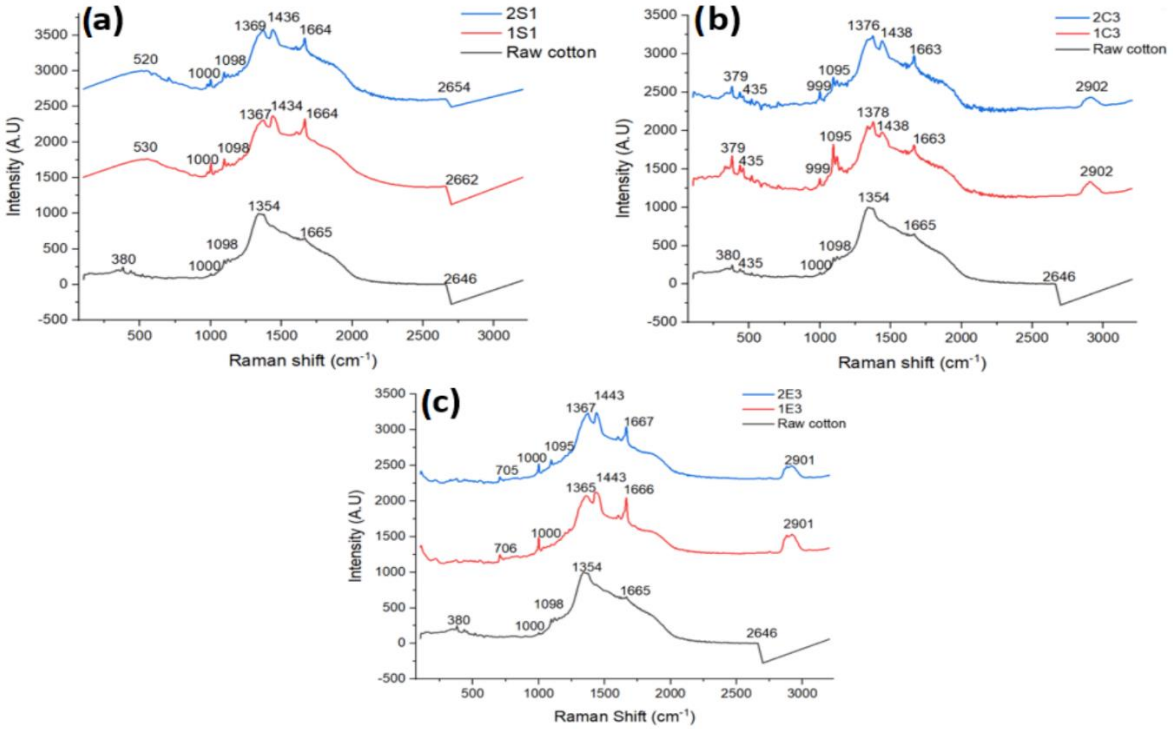



Figure 2.8. Raman spectra of CNC samples obtained through (**a**) $H_2SO_4$ hydrolysis; (**b**) HCl and (**c**) Enzymatic hydrolysis along with raw cotton.

Raman spectroscopy gives a molecular "fingerprint" that characterizes the cellulose nanomaterials by crystallinity, sulfate esters, and cellulose II. The characteristic Raman peaks related to specific molecular vibrations for the CNC samples obtained via $H_2SO_4$, HCl, and enzymatic hydrolysis were:

**$H_2SO_4$ Hydrolysis:** Peaks at 520–530 $cm^{-1}$ indicate glycosidic linkages and signals at ~1000 $cm^{-1}$ and 1100 $cm^{-1}$ correspond to C-C, C-O stretching, and cellulose ethers. Vibrations at 1337–1378 $cm^{-1}$ and deformation intensities at ~1434 $cm^{-1}$ reflect $CH_2$ bending, while amide bonds (~1664 $cm^{-1}$) suggest pectin residues.
**HCl Hydrolysis:** Peaks at 435–379 $cm^{-1}$ are due to cellulosic ring deformation. A similar stretching and bending pattern were observed at ~1000 $cm^{-1}$, 1374–1380 $cm^{-1}$, 1438 $cm^{-1}$, while CH stretching was seen at ~2900 $cm^{-1}$.
**Enzymatic Hydrolysis:** Unique peaks at ~700 $cm^{-1}$ highlight enzyme residues. Other peaks, such as ~1000 $cm^{-1}$, 1095 $cm^{-1}$, and 1443 $cm^{-1}$, are in agreement with S and C samples. The amide bonds (~1666 $cm^{-1}$) and CH stretching (~2901 $cm^{-1}$) are also noted.
All spectra confirm the formation of cellulose ether, partial removal of lignin, and efficiency in the extraction of CNC from cotton. Raman and FTIR data collectively validate the structural integrity and purity of CNCs.

## 2.10.4. XRD

XRD results indicated that all the CNC samples had peaks of crystalline cellulose, which were of higher intensity at the plane (002) at 22.5° and plane (101) at 14.7°, thus proving a higher degree of crystallinity compared to the raw cotton sample. Calculation of crystallinity percentage by the integration and Segal's method indicated variation among samples prepared via different hydrolysis and bleaching methods.

**$H_2SO_4$ Hydrolysis:** Sample S1 showed higher crystallinity (72.4%) than 2S1 (67.8%) through the integration method, suggesting that the 1st bleaching method is more effective than the 2nd one.
**HCl Hydrolysis:** Sample 2C3 had slightly greater crystallinity (76.4%) than 1C3 (73.1%), consistent with Segal's method results (89.1% vs. 87.9%).
**Enzymatic Hydrolysis:** Sample 2E3 showed higher crystallinity (75.1%) than 1E3 (63.5%), with Segal's method yielding around 84%, comparable to literature values for enzymatic hydrolysis from sugarcane bagasse.
Results show that bleaching methods have a significant impact on crystallinity, in which the 2nd method was more effective for HCl and enzymatic samples, while the 1st method was better for the $H_2SO_4$ samples.

**Table 5.** % crystallinity of samples by using integration and Segal's method.

| | % Crystallinity | |
|---|---|---|
| **Samples** | **Integration Method** | **Segal's Method** |
| $1S_1$ | 72.4 | 86.2 |
| $2S_1$ | 67.8 | 82.0 |
| $1C_3$ | 73.1 | 87.9 |
| $2C_3$ | 76.4 | 89.1 |
| $1E_3$ | 63.4 | 84.9 |
| $2E_3$ | 75.1 | 84.6 |
| Raw cotton | 40.6 | 81.0 |

$$\%\text{Crystallinity} = \frac{\text{area under the crystalline peaks}}{\text{area under all peaks}} \times 100$$

$$\%\text{Crystallinity} = \frac{I(\text{Crystalline}) - I(\text{Amorphous})}{I(\text{Crystalline})} \times 100$$

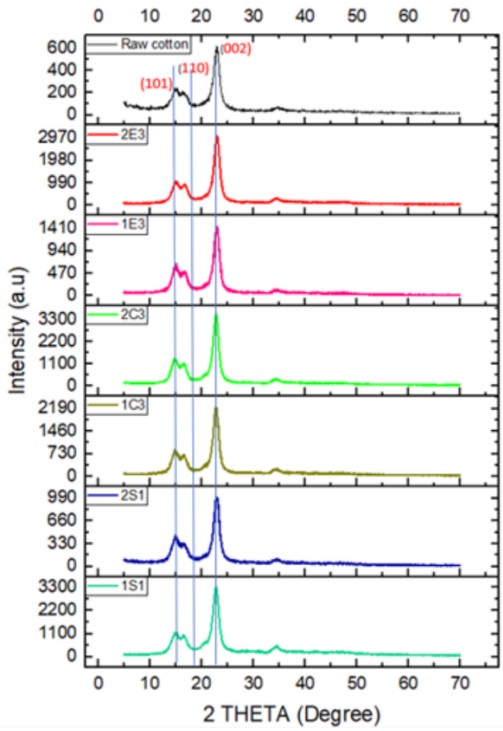


Figure 2.9. X-ray diffraction spectra of all CNC samples and raw cotton, respectively.

## 2.10.5. Scanning Electron Microscopy (SEM)

The SEM analysis represents the morphology of the CNC samples derived from raw cotton and through enzymatic and acid hydrolysis methods:

**Raw Cotton:** In its raw state, unbleached raw cotton demonstrated long, smooth fibrillar structures.

**Enzymatic Hydrolysis:** The samples (1E3, 2E3) had reduced fibril sizes and were partly fractionated to individual fibrils but remained long. The 2E3 sample showed increased fractionation compared to the 1E3 sample; NaOCl was more effective as a bleaching agent compared to $H_2O_2$. Since there was no complete breaking of the fibers, the produced samples here were cellulose nanofibrils with a rough/coarse structure.

**$H_2SO_4$ Hydrolysis:** The samples 1S1, 2S1 had rough, wrinkled surfaces with clear needle-like structures, which confirmed that both bleaching processes had effectively removed the lignin and hemicellulose.

**HCl Hydrolysis:** Samples (1C3, 2C3) had retained rod-like structures on the fibril surfaces and the cellulose was relatively intact. The fibrils were long, similar to the enzymatic hydrolysis samples.

The study revealed that bleaching and hydrolysis are processes that significantly alter the morphology, with enzymatic treatments yielding CNF and acid hydrolysis producing CNC with distinct structural features.

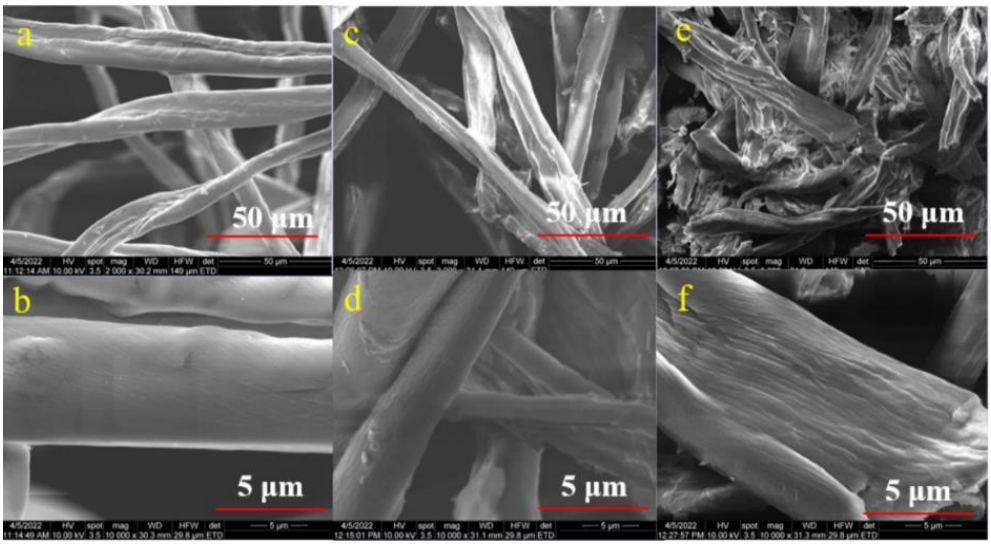



Figure 2.10. SEM Micrograph of the samples (a, b) raw cotton (c, d) $1E_3$, (e, f) $2E_3$.

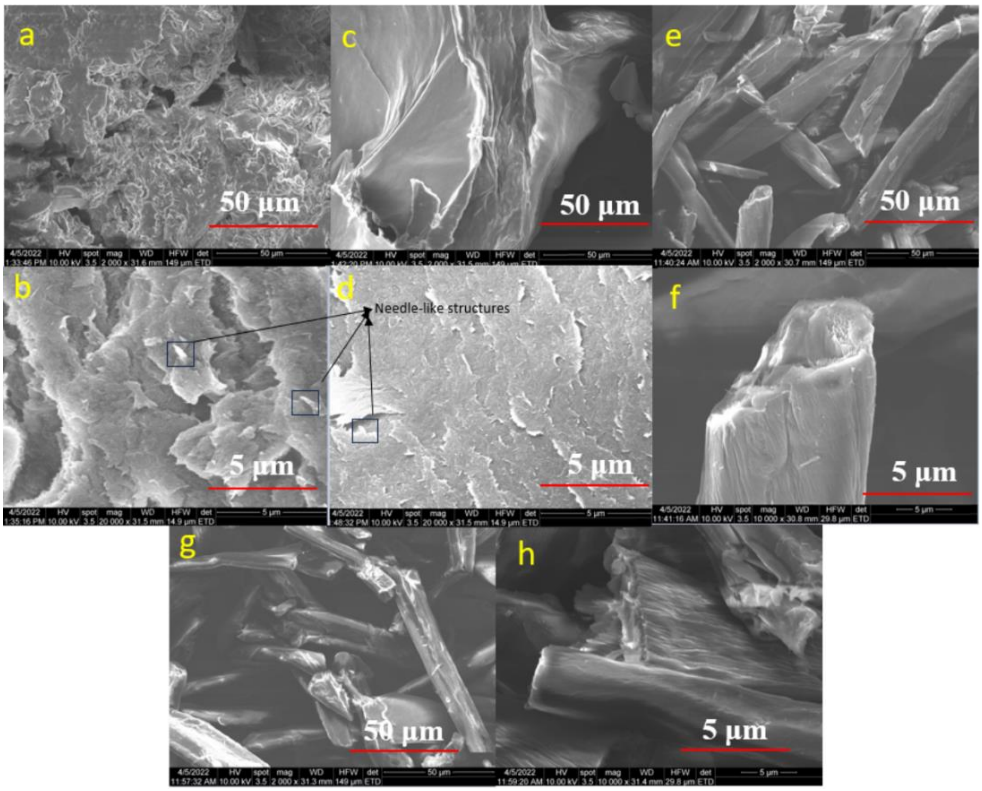



Figure 2.11. SEM Micrograph of the samples (a, b) $1S_1$, (c, d) $2S_1$, (e, f) $1C_3$, (g, h) $2C_3$.

## 2.10.6. TG Analysis

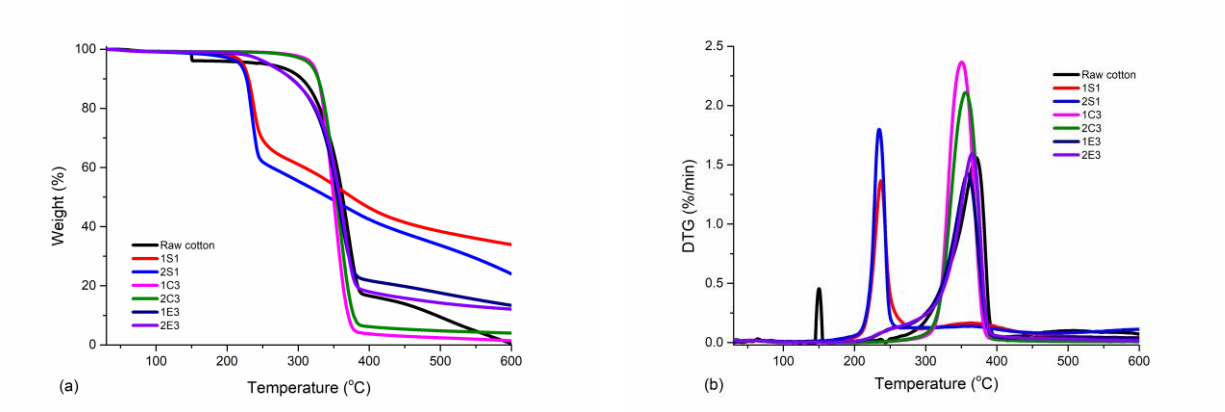



Figure 2.12. (a) TGA and (b) DTG profiles of the synthesized samples along with raw cotton.

Table 6. Percentage decomposition of samples at different temperatures.

| Samples | $T_{d3\%}$ (°C) | $T_{d5\%}$ (°C) | $T_{d10\%}$ (°C) | $T_{max}$ (°C) from DTG | Mass Loss (%) |
|---|---|---|---|---|---|
| Raw cotton | 150 | 255 | 305 | 375 | 99.57 |
| $1S_1$ | 214 | 222 | 230 | 236 | 66.16 |
| $2S_1$ | 202 | 218 | 227 | 235 | 76.17 |
| $1C_3$ | 309 | 320 | 329 | 350 | 98.62 |
| $2C_3$ | 302 | 317 | 328 | 355 | 96.02 |
| $1E_3$ | 241 | 259 | 291 | 358 | 86.69 |
| $2E_3$ | 241 | 259 | 290 | 364 | 87.93 |

The raw cotton sample showed significant weight loss due to absorbed water at 150 °C, complete degradation at 600 °C, and less than 0.5% residue. Samples 1S1 and 2S1 exhibited an early weight loss due to water and volatile compounds up to 100 °C, while the degradation started between 202-230 °C. Residues at 600 °C were 34% and 24%, respectively, related to sulfate groups, which accelerated the decomposition at low temperatures but possibly acted as flame retardants.

The degradation onsets for samples 1C3 and 2C3 were at higher temperatures: 300-328 °C, with very small residue values of 1.4% and 4%, respectively, proving complete removal of the inorganic acids. Samples 1E3 and 2E3 showed onsets between 241-291 °C, with residues of 13% and 12%, respectively, probably due to the presence of sodium citrate during the enzymatic treatments. Overall, the sulfation reaction negatively affected thermal stability; however, the possible flame-retardant capacity should be further investigated.

2.10.7. DSC Analysis

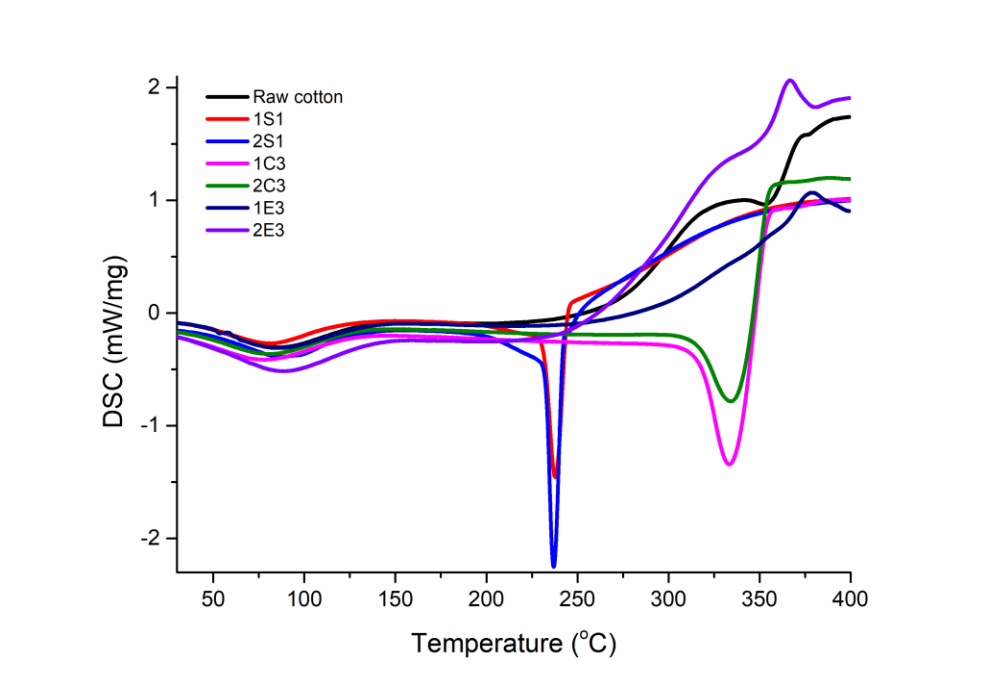



Figure 2.13. DSC profiles of all synthesized samples.

Table 7. The most important thermal parameters extracted from DSC analysis of all samples.

| Samples | $T_d$(°C) [a] | $\Delta H_{Td}$(J/g) [b] | $T_m$ (°C) [c] | $\Delta H_m$(J/g) [d] |
|---|---|---|---|---|
| Raw cotton | 86.1 | 74.9 | 352.3 | 37.4 |
| $1S_1$ | 81.8 | 47.6 | 237.6 | 70.4 |
| $2S_1$ | 86.3 | 52.1 | 236.8 | 72.1 |
| $1C_3$ | 77.4 | 52.2 | 333.4 | 232.9 |
| $2C_3$ | 80.7 | 61.7 | 334.3 | 208.1 |
| $1E_3$ | 86.2 | 65.1 | - | - |
| $2E_3$ | 86.1 | 80.0 | - | - |

(a—dehydration temperature; b—enthalpy of dehydration; c—melting point of the crystalline region of CNC; d—enthalpy of melting).

The DSC analysis highlights the thermal behavior of nanocellulose samples: S, C, and E. All samples showed an endothermic peak at approximately 80 °C, related to water evaporation, which is typical for cellulosic materials due to hydroxyl-water interactions. Samples processed with NaOCl bleaching presented higher water-loss temperatures and enthalpies than $H_2O_2$ bleached samples.

Crystalline melting points were recorded for cellulose at 237 °C in S samples and at 333 °C in C samples, the latter being significantly higher because sulfate groups decreased the activation energy of decomposition. No melting peaks were recorded for E samples, where exothermic peaks occurred at 381 °C (1E3) and 365 °C (2E3) due to molecular rearrangement. The differences in water content and enthalpy of dehydration of the E samples suggest that hydrolysis and bleaching significantly influence the thermal properties of nanocellulose.

## 2.11. Conclusions of the 1st study

In this work, hydrogen peroxide and sodium hypochlorite bleaching were used to extract cellulose nanomaterials, namely CNC and CNF, from raw cotton. Acid and enzymatic hydrolysis resulted in morphological, thermal, and structural differences. By SEM, the transition of the fiber bundles into CNC particles with wrinkles and needle-like structures was observed on S samples. FT-IR and Raman spectra showed the partial removal of lignin and hemicellulose.

$H_2O_2$ bleaching resulted in a more negative zeta potential of particles than the NaOCl method (−42 mV for 1S1 versus −32.8 mV for 2S1). Crystallinity was between 67.8–76.4% (integration method) and 82–89% (Segal's method). Bleaching with NaOCl had a greater impact on crystallinity and morphology compared to $H_2O_2$ bleaching. TGA showed that samples C and E exhibited better thermal stability compared to S samples. The study showed that the hydrolysis and bleaching methods highly affected crystallinity, morphology, and hydrodynamic properties, whereas thermal stability was less affected.

# CHAPTER 3

## CNC Modification with Acrylic acid and Furfuryl Amine Through Diels-Alder and Michael Addition Reactions

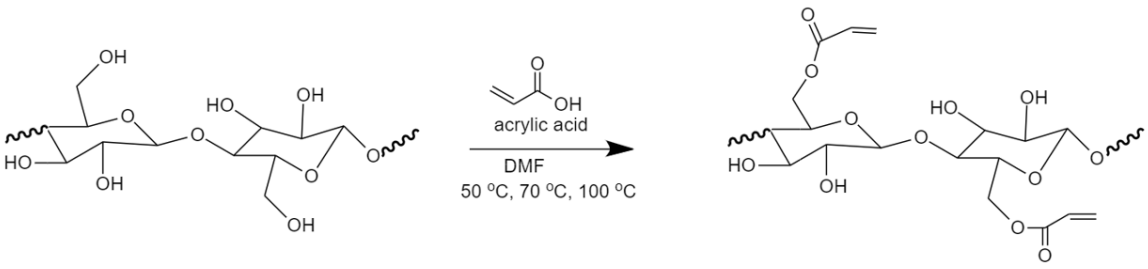
## 3.1. Objectives of the research study

This work aims to develop a new chemical modification of CNC to enhance hydrophobicity and increase the dispersibility of nanocrystals in organic solvents by grafting acrylic acid onto the surface of the CNC through esterification, followed by the reaction of furfuryl amine in Diels-Alder and Michael addition reactions. The overall aim is to improve compatibility and functionality in hydrophobic matrices while maximizing the unique chemical properties and surface reactivity of CNCs.

### 3.1.2. Chemical modification of CNC with Acrylic acid (CNC-AA) and Reaction of CNC-AA with Furfuryl amine

The described reactions outline a two-step chemical modification of cellulose nanocrystals (CNCs):

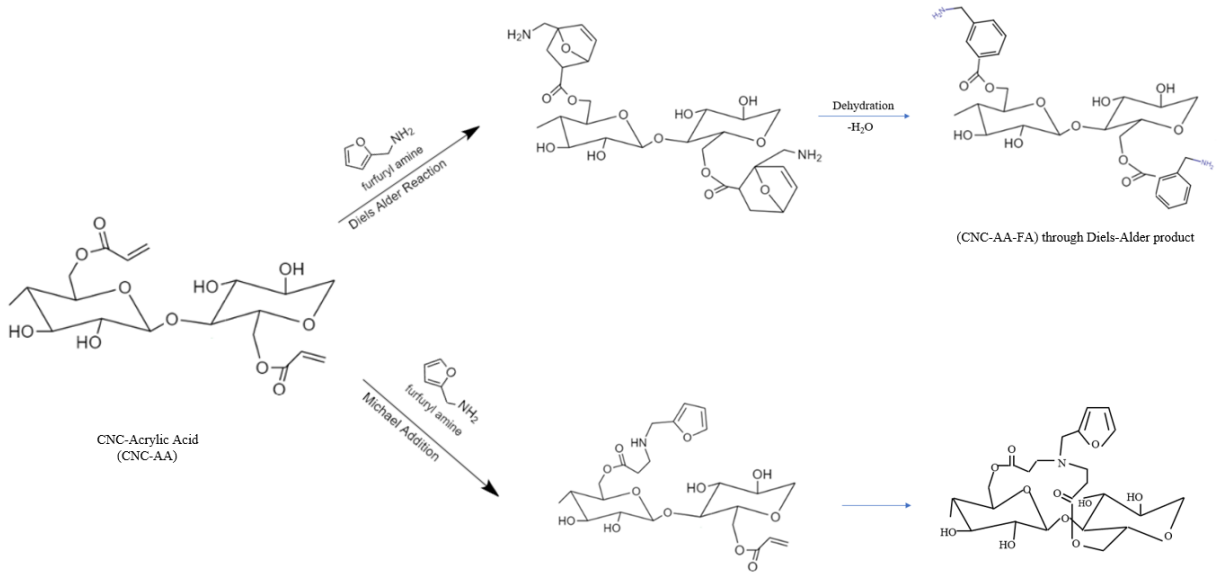
1. **Acrylic Acid Grafting (CNC-AA):**
    - CNC (1 g) was dispersed in 60 mL of DMF in a two-neck flask under a nitrogen atmosphere to prevent acrylic acid polymerization by free radicals.
    - Acrylic acid (0.4 mL) and concentrated $H_2SO_4$ (2 mL) were added as a catalyst, and the reaction was conducted at 100°C for 4 hours under constant stirring.
    - Post-reaction, the CNC-Acrylate (CNC-AA) product was separated by centrifugation, purified, and dried at room temperature.




CNC

CNC-Acrylic acid
(CNC-AA)

2. **Furfuryl Amine Functionalization (CNC-AA-FA):**
   - CNC-AA (0.3 g) was dispersed in 30 mL of DMF, followed by the addition of furfuryl amine (0.5 g) and $AlCl_3$ (0.1 g) as a Lewis acid catalyst.
   - The reaction was maintained at 60°C for 4 hours under constant stirring.
   - The final product, CNC-Acrylic Acid-Furfuryl Amine (CNC-AA-FA), was separated, washed to remove unreacted materials, and dried at room temperature.



## 3.7. Results and discussion

### 3.7.3. Fourier Transformed Infrared Spectrometry (FT-IR)

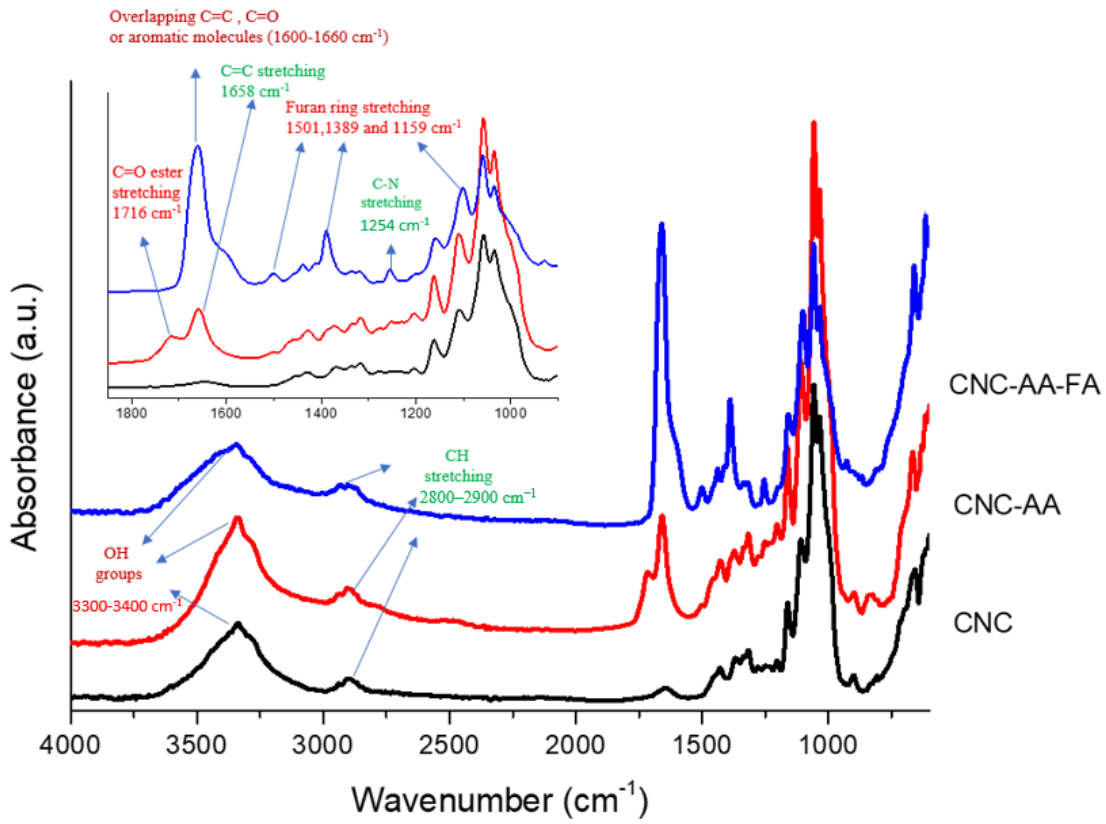



Figure 3.9. FTIR spectra of neat CNC, CNC-AA and CNC-AA-FA samples

FT-IR spectra analysis of cellulose nanocrystals and modified CNC samples reveals significant changes in the chemical structure after modification. Key observations from this analysis are summarized below:

**Common for All Samples:**

- Peaks at **3400–3300 $cm^{-1}$** correspond to OH stretching and bending vibrations.
- Peaks at **2900–2800 $cm^{-1}$** correspond to CH stretching.
- The **1400 $cm^{-1}$** peak corresponds to CH2 bending vibration, representing the crystalline band of cellulose.

**CNC Sample:**

- **1204 $cm^{-1}$**: Hemicellulose's acetyl group (-COO).
- **1057 and 1162 $cm^{-1}$**: C–O stretching vibrations.
- **1109 $cm^{-1}$**: Saccharide ring bending vibrations.
- **1360, 1280, and 1204 $cm^{-1}$**: CH bending vibrations.

**Sample CNC-AA:**

- Major peaks at **1716 $cm^{-1}$** of the C=O ester bond and **1658 $cm^{-1}$** C=C stretching confirm successful AA grafting.

**Sample CNC-AA-FA:**

- A disappearing or overlapping peak at **1716 $cm^{-1}$** with a strong peak around **1660 $cm^{-1}$** in the spectra confirms to its modification with FA.
- Peaks at **1501 $cm^{-1}$** due to furan ring stretching and **1159 $cm^{-1}$** due to -C-O-C- ether stretching confirm the presence of furan groups.
- Characteristic signals from **1600–1660 $cm^{-1}$**, **1500 $cm^{-1}$**, and **1389 $cm^{-1}$** are associated with the aromatic furan ring structure.
- The peak at **1254 $cm^{-1}$** can be assigned to C-N stretching, indicating reaction via Michael addition.
- Expected peaks for primary amines in the **3400–3250 $cm^{-1}$** range are not well defined, likely due to overlapping with OH groups on the cellulose surface.

These spectral changes and characteristic peaks confirm the successful chemical modifications of CNCs with AA and FA in this study.

### 3.7.4. X-ray Photoelectron Spectroscopy (XPS)

*Table 1*

**Elemental composition of CNC and its derivatives**

| Sample | C at. % | O at. % | N at. % |
|---|---|---|---|
| CNC | 61 | 39 | - |
| CNC-AA | 62 | 38 | - |
| CNC-AA-FA | 57 | 35 | 8 |

XPS analysis of the elemental composition of CNC, CNC-AA, and CNC-AA-FA samples showed that the modification with acrylic acid and furfuryl amine was successful. The carbon fraction increased from 61% to 62%, while oxygen decreased slightly from 39% to 38%. This indicates effective reaction of acrylic acid with OH groups on the CNC surface. Further reduction of carbon and oxygen percentages was obtained by the incorporation of nitrogen atoms derived from furfuryl amine.This indicates that furfuryl amine successfully reacted with the acrylic groups of CNC-AA, possibly through Diels-Alder or Michael Addition reactions.

There are distinct C1s, O1s, and N1s peaks for CNC-AA-FA, while for CNC and CNC-AA, only C1s and O1s peaks are present. The presence of the N1s peak testifies to the attachment of furfuryl amine. Deconvolution resulted peaks at 288.0 eV for C=N/C=O, 286.5 eV for C-O/C-N, 284.8 eV for C-C/C-H, and 284.5 eV for C=C. These results confirm the successful surface modifications of CNC with both acrylic acid and furfuryl amine.

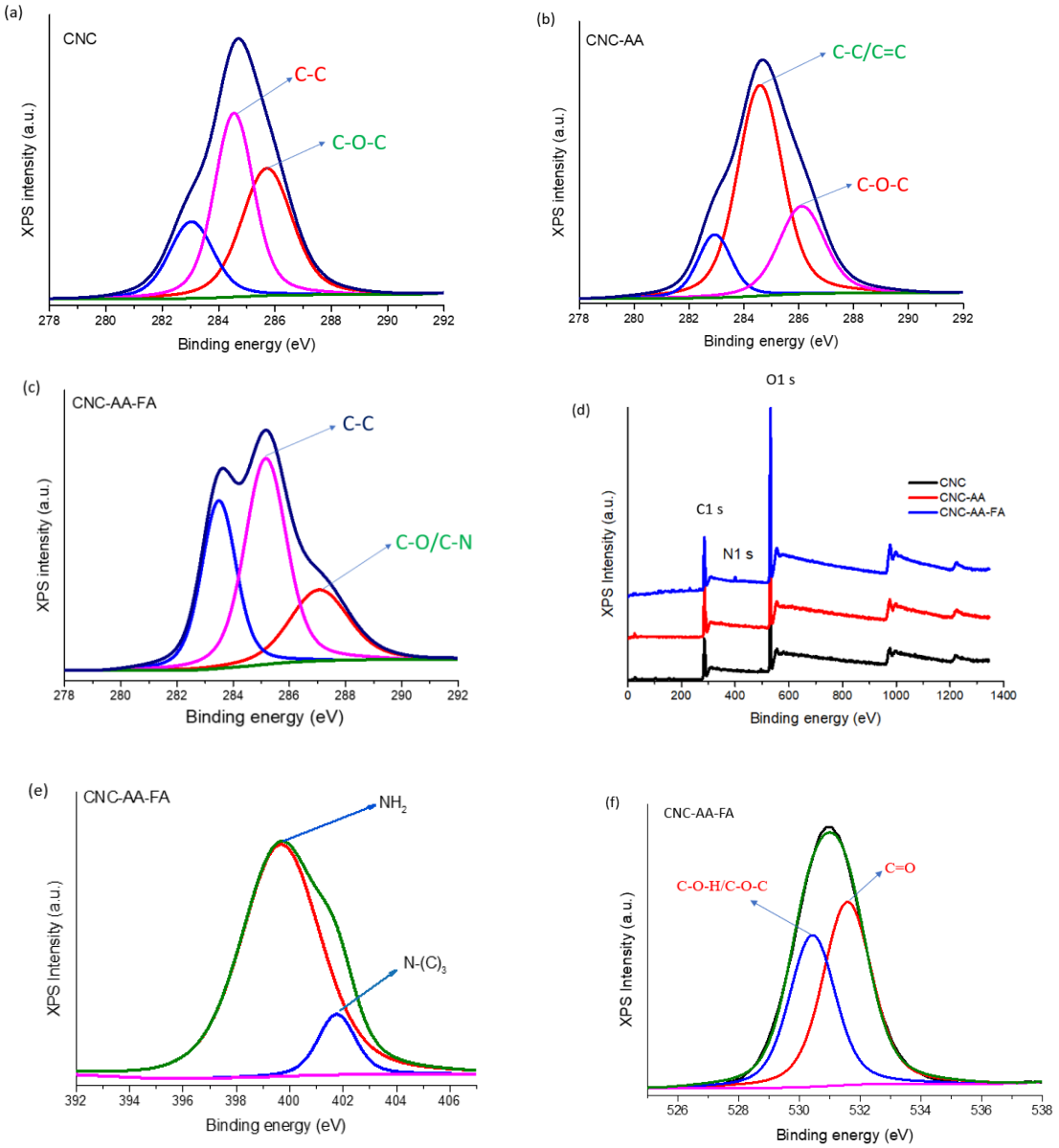



Figure 3.10. High-resolution C1s spectral deconvolution from XPS of a) neat pure CNC b) CNC-AA c) CNC-AA-FA derivatives and d) full range of XPS spectra of all samples e) The deconvolution of N1s spectra of CNC-AA-FA f) The deconvolution of O1s spectra of CNC-AA-FA

### 3.7.5. Thermogravimetric analysis (TGA)

*Table 2*

**Thermal parameters for CNC and its derivatives**

| Sample | $T_{d3\%}$ (°C) | $T_{d5\%}$ (°C) | $T_{d10\%}$ (°C) | $T_{d30\%}$ (°C) | $T_{max}$ (from DTG) | Residual mass (%) |
|---|---|---|---|---|---|---|
| CNC | 273.1 | 284.2 | 291.7 | 303.4 | 305.8 | 20.65 |
| CNC-AA | 71.6 | 93.8 | 202.6 | 257.3 | 258.2 | 22.14 |
| CNF-AA-FA | 55.2 | 64.3 | 81.4 | 215.3 | 263.7 | 25.02 |

TGA thermograms of CNC, CNC-AA, and CNC-AA-FA samples have revealed distinct behaviors of the thermal properties of the samples.

**CNC Sample:**

- The initial 3% weight loss due to the thermal disintegration of the amorphous phase, while crystalline degradation occurs at 273°C.
- Onset degradation temperature (Td10%): 292°C.
- Maximum degradation temperature: 306°C.
- Residual weight at 800°C: 21%.

**CNC-AA Sample:**

- Decreased thermal stability than neat CNC, Td10% of 203°C, maximum degradation temperature at 258°C.
- The reduced thermal stability is attributed to the presence of acrylate groups that accelerate the degradation of cellulose.
- The single peak in both TGA and DTG shows the covalent linkage of AA with CNC, with no by-products formed in between.

**CNC-AA-FA Sample:**

- Had two phases of thermal weight loss:
    1. First weight loss (around 90°C), which was due to degradation of furfuryl amine.
    2. Second weight loss (around 260°C) due to acrylic acid degradation.

These results show that chemical modifications with AA and FA affect the thermal stability and degradation patterns of CNCs.

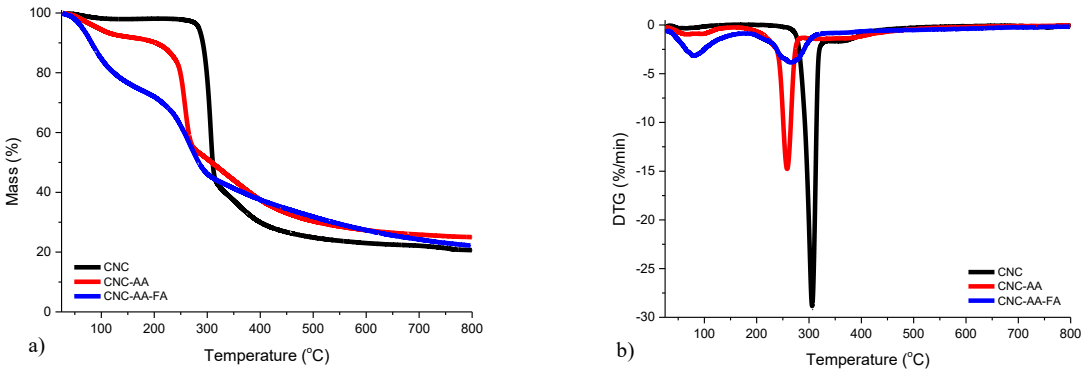



Figure 3.11. a) TGA curves and b) the derivative thermogravimetric curves (DTG) of each CNC samples in the range of 25°C - 600°C

### 3.7.6. Differential Scanning Calorimetry (DSC)

*Table 3*

**DSC data of CNC and its derivatives**

| Sample | $\Delta H_1$ (J/g) | $T_{max1}$ (°C) | $\Delta H_2$ (J/g) | $T_{max2}$ (°C) |
|---|---|---|---|---|
| CNC | 147.9 | 60.5 | 313.0 | 304.1 |
| CNC-AA | 175.4 | 75.6 | 240.5 | 277.4 |
| CNF-AA-FA | 210.9 | 78.0 | 227.8 | 287.0 |

DSC curves were used to complement the TGA results for the heat degradation of cellulose. Broad endothermic signals between 60–90°C indicate heat absorption due to water evaporation in all samples. Transition temperatures are important to determine the structural stability after heating. Neat CNC showed the highest degradation temperature of 304.1°C, which suggests that it is more thermally stable. CNC-AA-FA had a higher degradation temperature (287°C) than CNC-AA (277.4°C). Covalent modifications on CNC surfaces lower the transition temperatures compared to neat CNCs.

Differences in melting enthalpy reflect chemical modifications of the samples.
Thermal degradation between 200-300°C in the DSC curves is in line with TGA findings and reinforces the effect of chemical modification on thermal properties. This analysis underlines how chemical modification influences the thermal stability and the degradation behavior of CNCs.

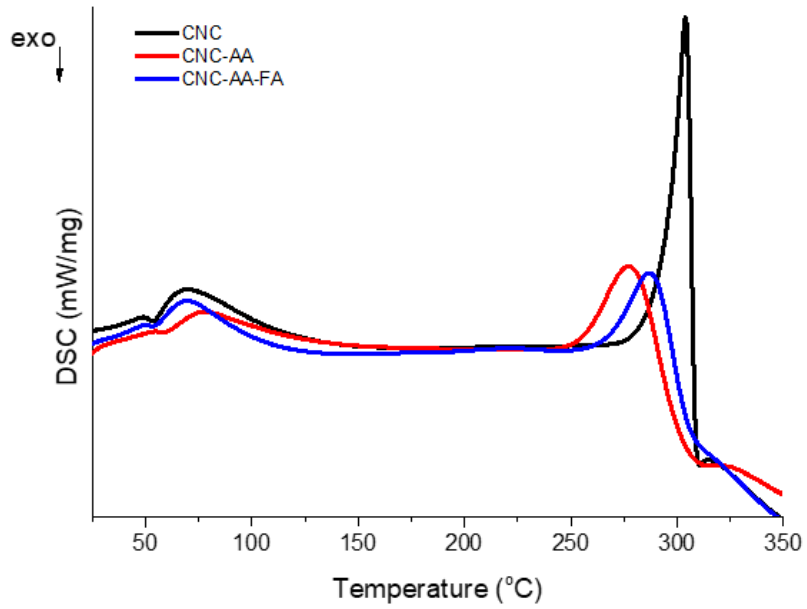



Figure 3.12. DSC curves of all samples.

### 3.7.7. Scanning Electron Microscopy (SEM)

The morphology of the CNC, CNC-AA, and CNC-AA-FA samples was investigated by SEM, revealing distinct structural changes before and after modification:

**Neat CNC:**

- SEM images (Figure 3.13.a and b) show that the commercial CNC sample has a **spherical morphology**, which differs significantly from the typical rodlike structure.

**CNC-AA:**

- Acrylic acid treatment induces **agglomeration**, forming a **stiffer and denser structure** (Figure 3.13.c and d).
- This agglomeration is attributed to the proximity of particles during solvent evaporation.

**CNC-AA-FA:**

- Further modification with furfuryl amine reduces the agglomerated structure, resulting in a **more irregular and non-uniform morphology** (Figure 3.13.e and f).
- The reduction in agglomeration is due to **hydrophobic interactions** provided by furfuryl amine on the CNC surface.

Agglomeration of CNC samples occurs during the acrylic acid reaction but is reduced by furfuryl amine modification, leading to less uniformity and decreased agglomeration.

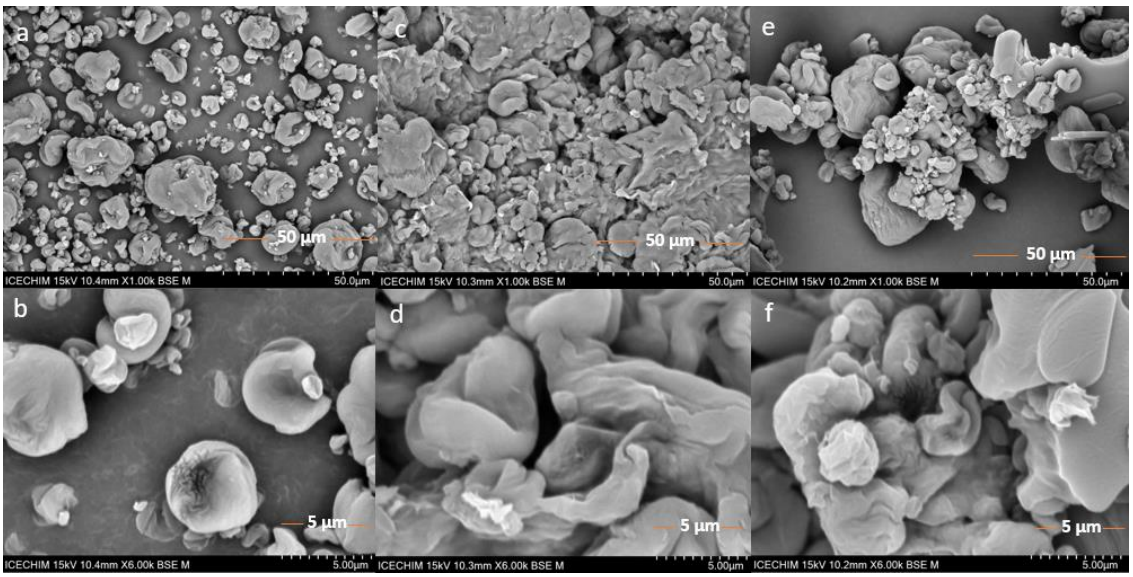



Figure 3.13. SEM samples of a,b) neat CNC c,d) CNC-AA  e,f) CNC-AA-FA

## 3.8. Conclusions of the 2nd Study :

**FT-IR Spectra Changes:**

- Significant changes between **1200 $cm^{-1}$ and 1800 $cm^{-1}$** were observed after CNC modification with acrylic acid (AA) and furfuryl amine (FA).
- **C=O** and **C=C stretching vibrations** confirmed the formation of CNC-AA, while characteristic furan ring bands at **1600–1660 $cm^{-1}$, 1500 $cm^{-1}$, and 1389 $cm^{-1}$** indicated successful CNC-AA-FA modification.

**Thermal Stability (TGA):**

- CNC-AA showed **lower thermal stability** than neat CNC due to the acrylate group accelerating degradation.
- The TGA of CNC-AA-FA demonstrated **two-step weight losses** at **90°C** and **260°C**, attributed to the decomposition of furfuryl amine and acrylic acid, respectively.

**Thermal Transition (DSC):**

- Modified CNC samples exhibited **lower Tmax** compared to neat CNC.
- This reduction could be due to an increase in **amorphous content** after chemical modification, as neat CNC is more crystalline.

**Elemental Composition (XPS):**

- XPS confirmed the successful modifications of **acrylic acid** and **furfuryl amine** on CNC surfaces, reflecting both **Diels-Alder** and **Michael addition reactions**.

**Morphology (SEM):**

- SEM analysis revealed changes in the **surface uniformity** of CNC due to functional groups introduced during chemical modification.

These results confirm that CNC underwent **chemical and structural modifications** with acrylic acid and furfuryl amine, altering its thermal properties, morphology, and surface chemistry.

# CHAPTER 4

Comparison of Solvent Casting and Pickering Emulsion Methods for Improving Mechanical Properties of PLA Composites in Packaging Application with SurfaceModified Cellulose Nanomaterial

## 4.1. Objectives of the research study

The aim of the study is to improve the mechanical and sustainable properties of biodegradable packaging materials; specifically, enhancing the properties of polylactic acid through the incorporation of modified and unmodified cellulose nanocrystals . The presented work focuses on surface modification techniques, including grafting 2,4-methylene diphenyl diisocyanate and castor oil, to improve the compatibility and dispersion of CNC within PLA matrices. This work aims to enhance the mechanical strength, flexibility, and thermal stability of PLA composites. Additionally, two different methods of nanocellulose incorporation into composite materials are compared: Solvent casting and Pickering emulsion. These methods are compared based on their efficiency in improving the dispersion and compatibility of nanocellulose in hydrophobic polymer matrices to achieve better performance and, ultimately, stronger and more sustainable biopolymer-based materials.

### 4.6.1. Grafting of MDI onto the CN surface

2 g of dried CNC were dispersed in 50 mL of anhydrous toluene and sonicated for 10 minutes at 50% amplitude (20–40 kHz). 4 g of MDI were added, and the reaction was carried out at 80 °C for 4 hours under nitrogen. The mixture was centrifuged at 9000 rpm to isolate CNC-MDI, rinsed five times with dry toluene, and dried at 25 °C, yielding 2.1 g of CNC-MDI.

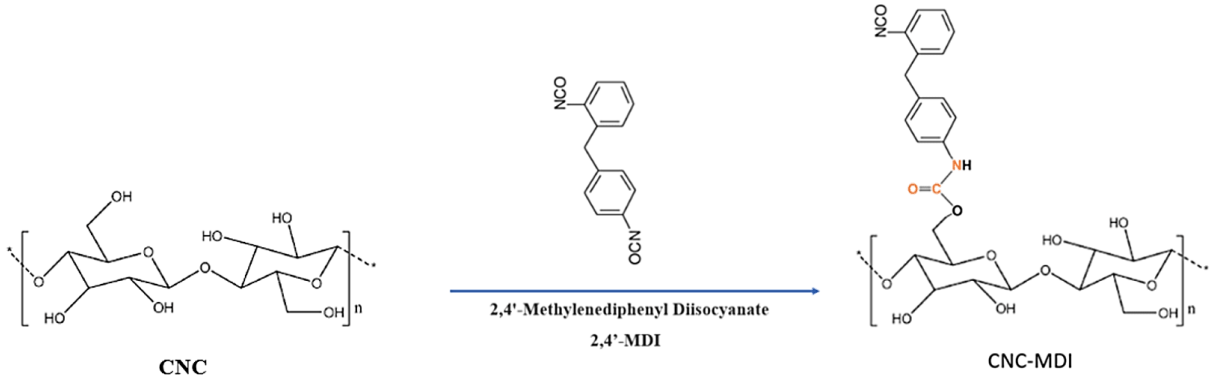



Figure 4.4. Reaction between CNC and MDI.

### 4.6.2. Grafting of NCO-terminated CN-MDI with castor oil

1.5 g of CNC-MDI was dispersed in 50 mL of anhydrous toluene via 10 minutes of sonication at 50% amplitude. After dispersion, 4.5 g of castor oil and 0.3 mL of dibutyltin dilaurate (DBTL) were added, and the reaction was conducted at 80 °C for 15 hours. The resulting mixture was centrifuged to isolate CNC-MDI-CO, washed with toluene, and dried.

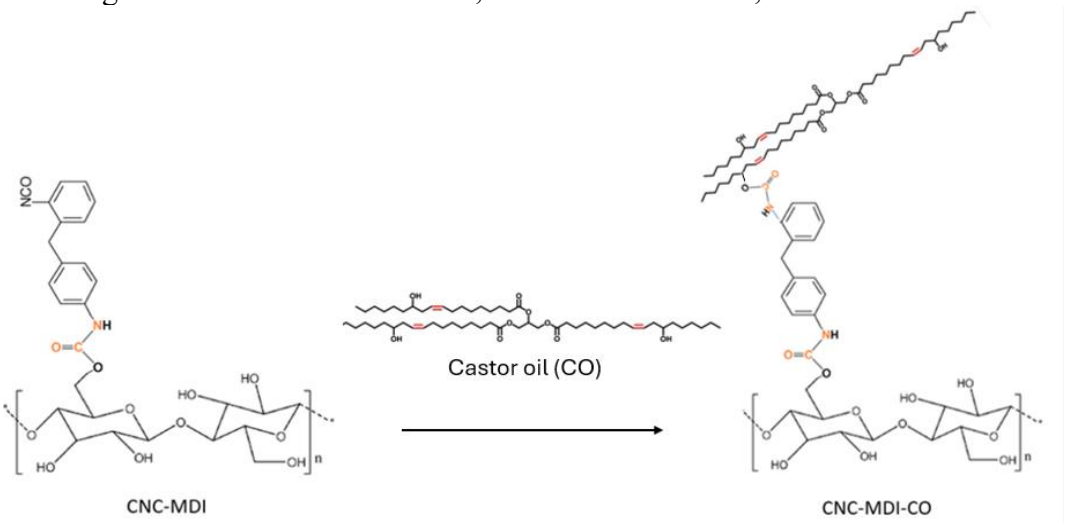



Figure 4.5. Reaction between modified CNC and Castor oil.

### 4.6.3. PLA-CNC-Based Nanocomposite Synthesis

Two methods, **solvent casting** and **Pickering emulsion**, were employed to synthesize PLA nanocomposites with CNC and CNC-MDI-CO:

1. **Solvent Casting:**
    - **Process:**
        - Dissolve 4 g of PLA in 100 mL toluene.
        - Disperse CNC or CNC-MDI-CO (1, 3, or 5 wt.% of PLA) in 25 mL toluene and sonicate for 10 minutes in an ice bath.
        - Mix both solutions, sonicate for another 10 minutes, and cast onto a Petri dish.
        - Dry the films at room temperature for 24 hours.
2. **Pickering Emulsion:**
    - **Process:**
        - Dissolve 4 g of PLA in 100 mL dichloromethane (DCM) to form the organic phase.
        - Disperse CNC and CNC-MDI-CO in water to form the aqueous phase.
        - Mix both phases at a shear rate of 2000 $s^{-1}$ for 1 hour at 25 °C.
        - Transfer the emulsion into a Petri dish and air-dry for 24 hours.
        - As DCM evaporates, PLA/CNC composite microspheres are obtained.
        - Use compression molding (180 °C, 15,000–20,000 N for 5 minutes) to form a uniform PLA/CNC composite.

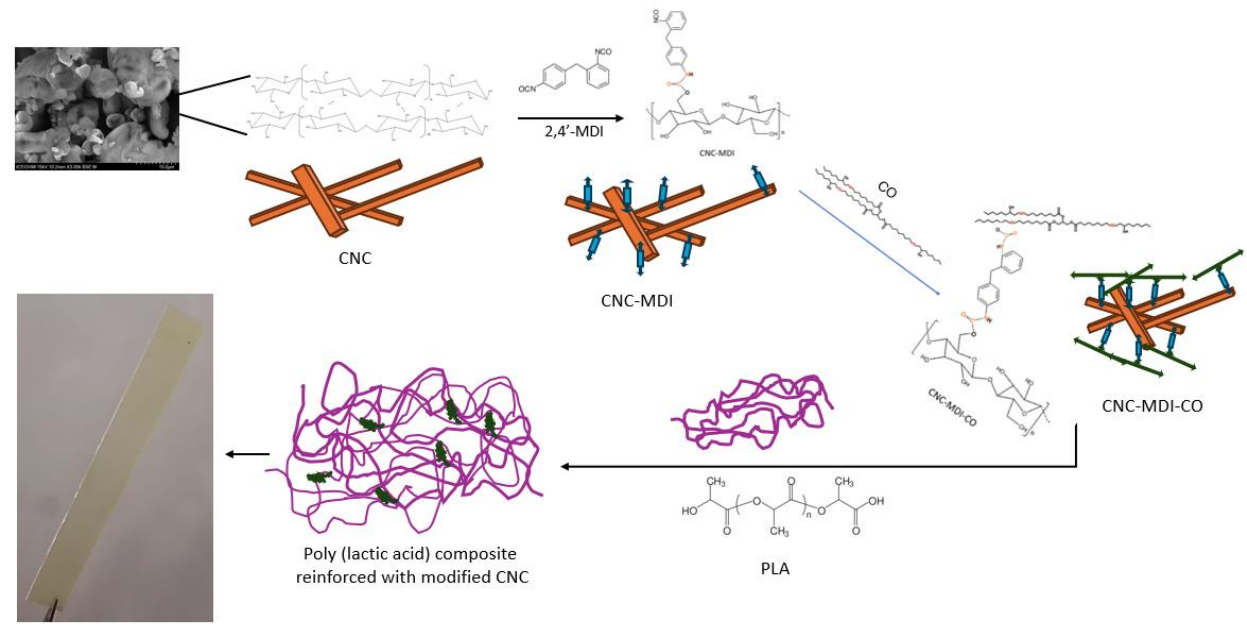



Figure 4.6. Schematic representation of CNC modification and PLA nanocomposite preparation.

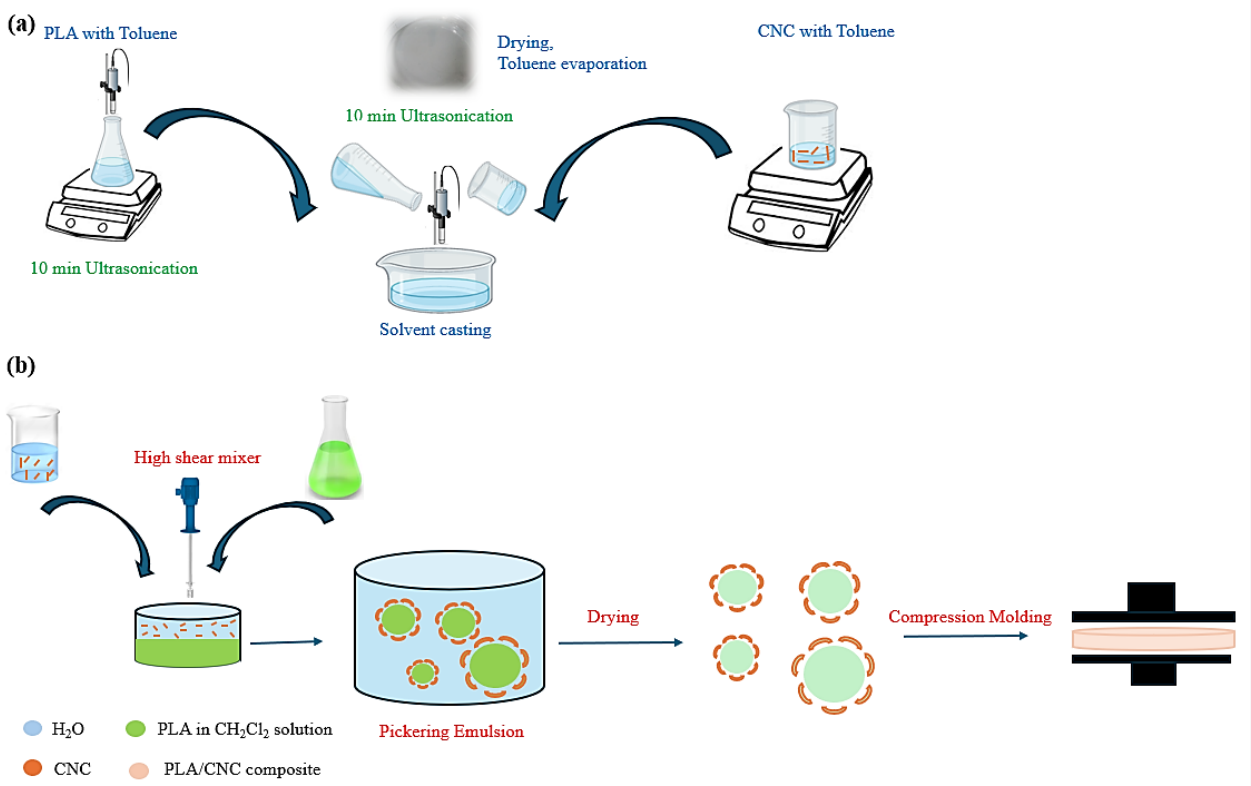



Figure 4.7. Schematic illustration of the production of PLA-CNC composite films through (a) solvent casting and (b) Pickering emulsion.

## 4.8. Results and Discussion

### 4.8.1. FTIR Analysis of CNC and Modified CNC Samples

The FTIR spectra determined the chemical structure of unmodified and modified CNCs; the key observations are as follows:

**Unmodified CNC:**

- A broad peak at **3400–3300 $cm^{-1}$** corresponds to hydroxyl (OH) groups.
- Peaks at **2850–2950 $cm^{-1}$** relate to C-H stretching in the cellulose chain.
- The band near **1640 $cm^{-1}$** corresponds to water molecule bending.
- Peaks at **1119 $cm^{-1}$** and **1062 $cm^{-1}$** confirm the C-O bond structure of cellulose.

**CNC Modified with MDI (CNC-MDI):**

- A strong peak at **2270 $cm^{-1}$** indicates unreacted isocyanate (NCO) groups.
- A weak new peak at **1743 $cm^{-1}$** represents urethane C=O groups formed between MDI and cellulose.
- The cellulose structure remains mostly unchanged, with minimal alteration in hydroxyl, C-H, and C-O signals.

**CNC Modified with MDI and Castor Oil (CNC-MDI-CO):**

- A stronger peak at **2924 $cm^{-1}$** and a new peak at **2855 $cm^{-1}$** indicate C-H and $CH_2$ stretching from the alkyl chains of castor oil.
- A pronounced band at **1743 $cm^{-1}$** highlights the carbonyl (C=O) contribution from ester bonds in castor oil, distinguishing CNC-MDI-CO from CNC-MDI.

FTIR analysis confirmed the successful functionalization of CNC with MDI and subsequent modification with castor oil, maintaining the cellulose structure while incorporating new chemical groups specific to each modification.

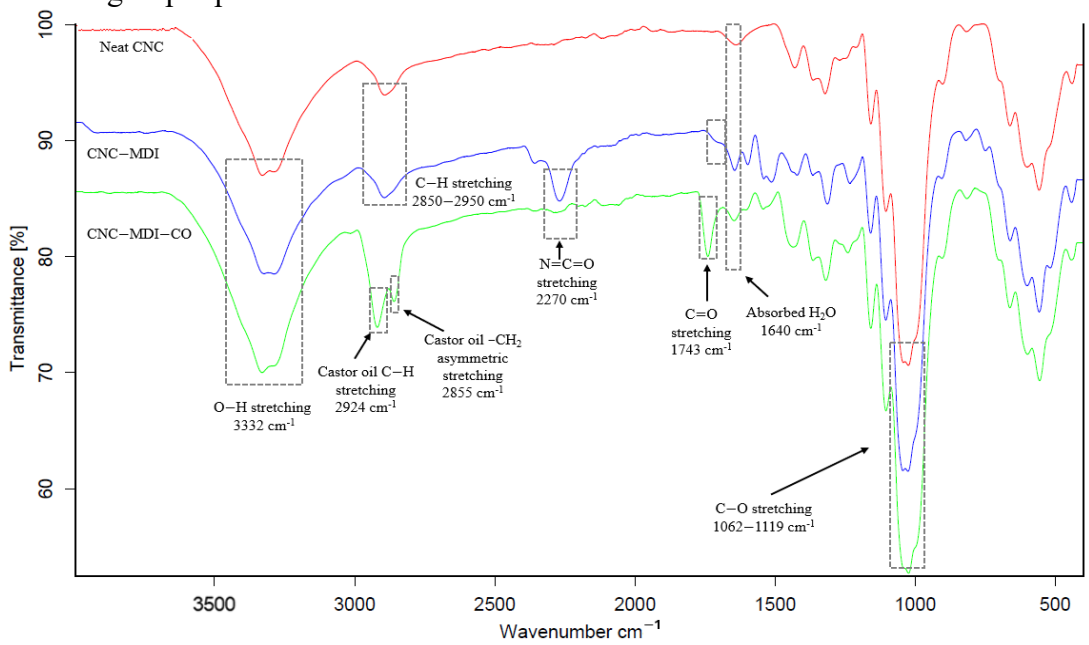



Figure 4.8. FTIR spectra of neat and modified CNC samples.

## 4.8.2. XPS Analysis of CNC and modified CNC samples

XPS analysis demonstrated the surface modification of the CNC with MDI and castor oil. The results reflected significant changes in the elemental composition, indicating the inclusion of nitrogen-containing isocyanate groups and castor oil.

**Elemental Composition:**

Native CNC is primarily composed of carbon (64.1%) and oxygen (34.7%), with no detectable nitrogen.

Following modification with MDI, nitrogen appears at 5.8%, the carbon content rises to 80.8%, and oxygen decreases to 12.7%, confirming the reaction of MDI with hydroxyl groups on the CNC surface.

Further modification with castor oil (CNC-MDI-CO) raises the carbon content to 85.1%, while nitrogen decreases to 2.5% and oxygen to 12.4%. These changes validate the incorporation of new chemical groups.

**High-Resolution C1s Spectrum:**

- CNC exhibits peaks corresponding to C-H, C-C, and C-OH bonds.
- CNC-MDI introduces peaks associated with O-C=O ester bonds, indicating urethane formation.
- CNC-MDI-CO shows an increased intensity of C-OH bonds, attributed to the additional OH groups provided by castor oil.

**High-Resolution O1s and N1s Peaks:**

- The O1s spectrum reflects changes in oxygen-containing groups: OH groups in CNC, carbonyl (C=O) groups in CNC-MDI, and ester or carboxylate groups in CNC-MDI-CO.

- N1s peaks observed in CNC-MDI and CNC-MDI-CO confirm successful modifications with MDI and castor oil.

**Additional Peaks:**

- The Sn3d peak observed in CNC-MDI-CO results from the use of dibutyltin dilaurate as a catalyst.

These findings confirm the successful chemical modifications, enhancing CNC's properties for specific applications.

Table 1: Elemental composition of CNC and modified CNC samples

| Sample | C at. % | O at. % | N at. % |
|---|---|---|---|
| Neat CNC | 64.1 | 34.7 | - |
| CNC-MDI | 80.8 | 12.7 | 5.8 |
| CNC-MDI-CO | 85.1 | 12.4 | 2.5 |

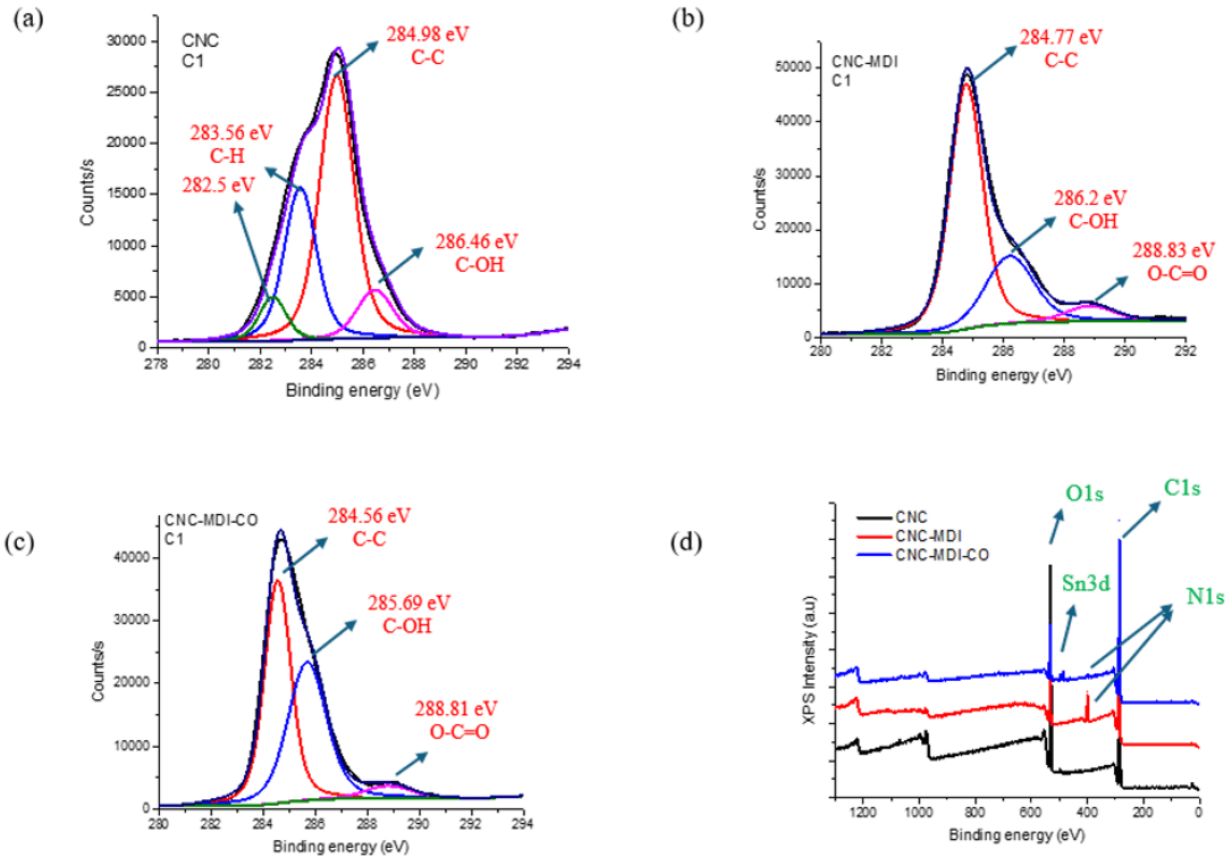



Figure 6. High-resolution C1s spectral deconvolution from XPS of (a) neat CNC (b) CNC-MDI (c) CNC-MDI-CO and (d) full range of XPS spectra of all samples

### 4.8.3. DSC Analysis of CNC and modified CNC samples

DSC data provides critical insights into the thermal properties of CNC and its modified forms, CNC-MDI and CNC-MDI-CO.

**CNC:**

- **$\Delta H_1$**: 47.09 J/g at **$T_{max1}$** = 69.4°C, likely due to moisture evaporation or slight decomposition.
- **$\Delta H_2$**: 263.9 J/g at **$T_{max2}$** = 304.1°C, indicating high thermal stability up to 304°C, beyond which the degradation rate increases.

**CNC-MDI (Modified with Isocyanate):**

- Energy absorption decreases in both phases:
  - **$\Delta H_1$** reduces to 11.81 J/g, while **$T_{max1}$** shifts slightly higher to 74.5°C, potentially due to cross-linking effects.
  - **$\Delta H_2$** reduces to 187.2 J/g, while **$T_{max2}$** remains almost unchanged at 305.2°C, preserving thermal degradation stability despite reduced energy absorption.

**CNC-MDI-CO (Modified with Isocyanate and Castor Oil):**

- **$\Delta H_1$** increases to 60.3 J/g, surpassing unmodified CNC, indicating a stronger endothermal effect during the first thermal phase.
- **$T_{max1}$** slightly decreases to 68.4°C, signaling an earlier thermal onset.
- **$\Delta H_2$** is 244.3 J/g at **$T_{max2}$** = 304.8°C, suggesting that while decomposition energy increases, thermal stability remains intact.

CNC-MDI-CO modification enhances heat absorption capacity without compromising thermal stability, making it advantageous for applications requiring improved thermal properties. Meanwhile, CNC-MDI demonstrates reduced energy absorption while retaining thermal degradation stability.

Table 2: Thermal parameters of samples for CNC and modified CNC samples

| Samples | $\Delta H_1$ (J/g) | $T_{max1}$ (°C) | $\Delta H_2$ (J/g) | $T_{max2}$ (°C) |
|---|---|---|---|---|
| Neat CNC | 47.09 | 69.4 | 263.9 | 304.1 |
| CNC-MDI | 11.81 | 74.5 | 187.2 | 305.2 |
| CNC-MDI-CO | 60.3 | 68.4 | 244.3 | 304.8 |

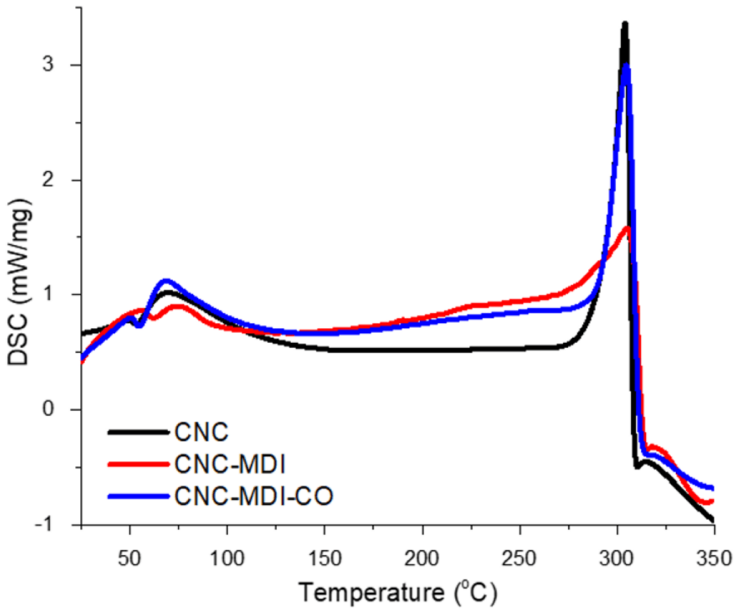


Figure 4.10. DSC profiles of CNC, CNC-MDI, and CNC-MDI-CO samples

### 4.8.4. TG Analysis of CNC and modified CNC samples

The analysis indicates that incorporating MDI and CO into CNC does not result in significant changes to its thermal stability.

**Thermal Degradation Temperature:**

- **Td3%**, **Td5%**, and **Td10%** values for CNC-MDI and CNC-MDI-CO are slightly lower than those of neat CNC, reflecting a minor reduction in thermal stability.
- These variations are within an acceptable range, confirming that surface modifications with MDI and CO have negligible impact on thermal stability.

**Maximum Decomposition Rates:**

- $\mathbf{T_{max}}$ values from DTG curves are nearly identical across all samples, indicating that the maximum thermal decomposition occurs within the same temperature range for both modified and unmodified CNC.

**Mass Loss Stability:**

- The mass loss percentages across all samples are comparable, reinforcing that the addition of MDI and CO does not significantly influence the thermal degradation behavior.

These findings demonstrate that surface modifications with MDI and CO introduce only marginal changes to the thermal stability and degradation behavior of CNC-based composites, consistent with similar studies in literature.

Table 3. Percentage decomposition of CNC and modified CNC samples.

| Samples | $T_{d3\%}$ (°C) | $T_{d5\%}$ (°C) | $T_{d10\%}$ (°C) | $T_{max}$ (°C) from DTG | Mass Loss (%) |
|---|---|---|---|---|---|
| Neat CNC | 233 | 279 | 290 | 305 | 79.6 |
| CNC-MDI | 218 | 264 | 288 | 308 | 78.6 |
| CNC-MDI-CO | 228 | 265 | 288 | 308 | 78.5 |

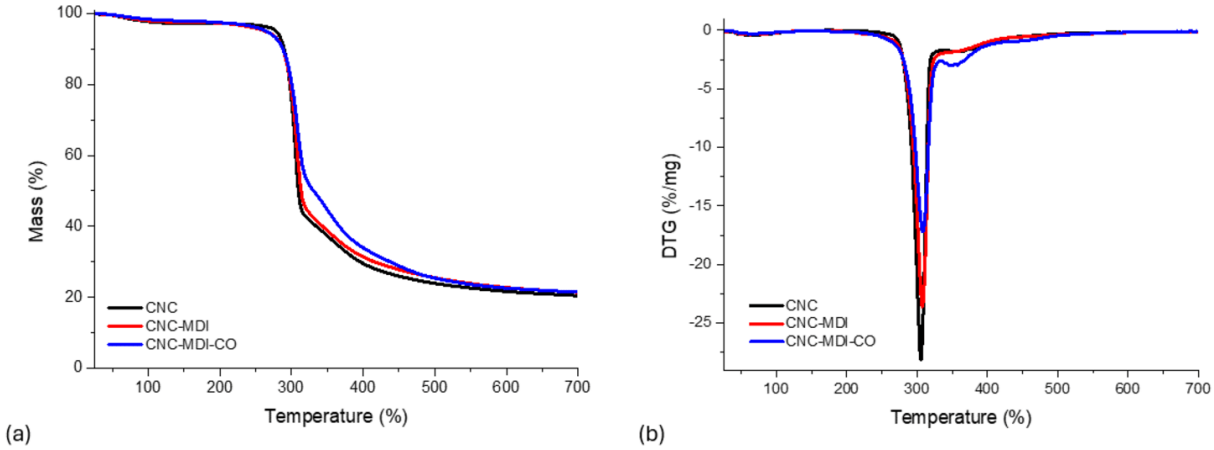



Figure 8. (a) TGA and (b) DTG curves for CNC and modified CNC samples.

## 4.8.5. Contact Angle (CA) Analysis of CNC and modified CNC samples

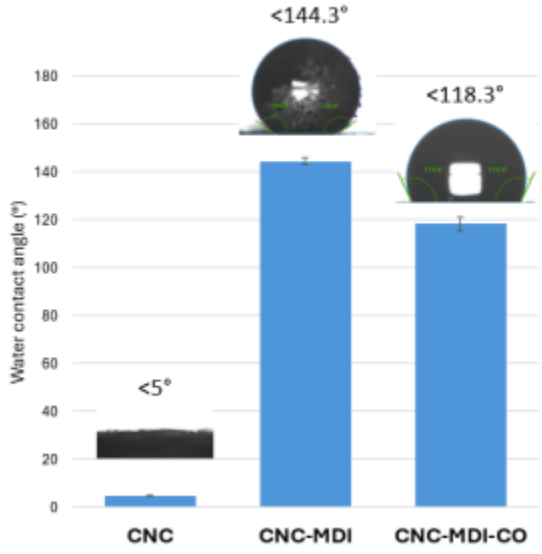



Figure 4.12. Water contact angle of CNC and modified CNC samples.

Figure 4.12 shows the water contact angle of the CNC and modified CNC samples to illustrate the change in wettability of the surface. The neat CNC, with hydrophilic hydroxyl groups on its surface, exhibited a contact angle less than 5°, indicating strong hydrophilicity. Chemical modification with MDI replaced these groups with hydrophobic urethane and phenyl groups, which increased the contact angle to 144.3° and enhanced hydrophobicity. Further functionalization with castor oil decreased the contact angle to 118.3° since hydroxyl groups were present in castor oil, reintroducing hydrophilic character and thereby decreasing the hydrophobicity of the surface as a whole.

### 4.8.6. SEM Analysis of CNC and modified CNC samples

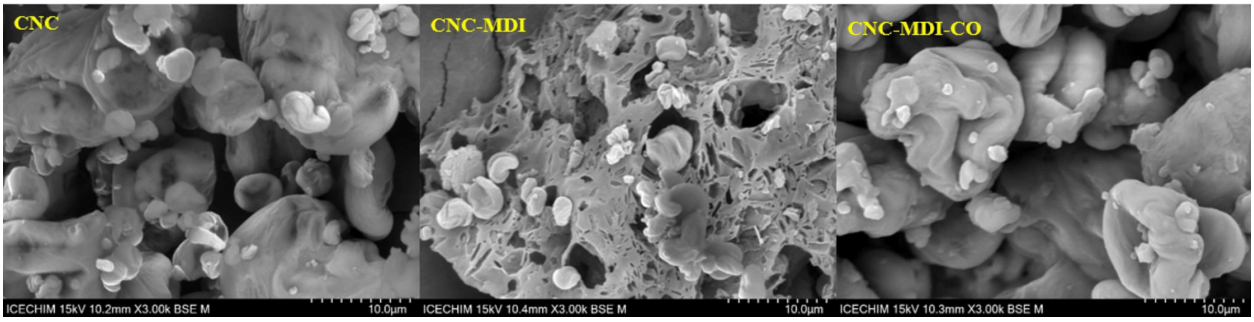



Figure 10. SEM samples of neat CNC, CNC-MDI and CNC-MDI-CO

Neat CNC displayed a spherical, aggregated structure with moderate porosity and a smooth surface, differing from the expected rod-like shape. This aggregation likely occurs due to capillary forces during the drying process, highlighting the need for optimized drying techniques, such as lyophilic drying or sequential solvent exchange, to preserve the rod-like morphology and improve dispersion.

The structure of CNC modified with MDI exhibited significant changes, including increased porosity, larger void spaces, and less compact clusters compared to neat CNC. These changes indicate that the interaction of MDI with CNC, involving surface roughening and cross-linking processes, resulted in a more open and irregular structure.

Further modification with castor oil produced a smoother surface and a more compact morphology, while still maintaining porosity and flexibility. The presence of castor oil within the CNC-MDI matrix appears to support the development of an elastic and flexible network.

Overall, SEM analysis reveals that treatments with MDI and castor oil considerably influence the surface roughness, porosity, and dispersion of CNCs. These modifications enhance mechanical properties such as elasticity and flexibility, while underscoring the structural changes resulting from chemical interactions. The findings emphasize the need to optimize drying and reaction processes to better control the final morphology and dispersion of CNC materials.

## 4.8.7. FTIR Analysis of CNC- PLA Nanocomposites

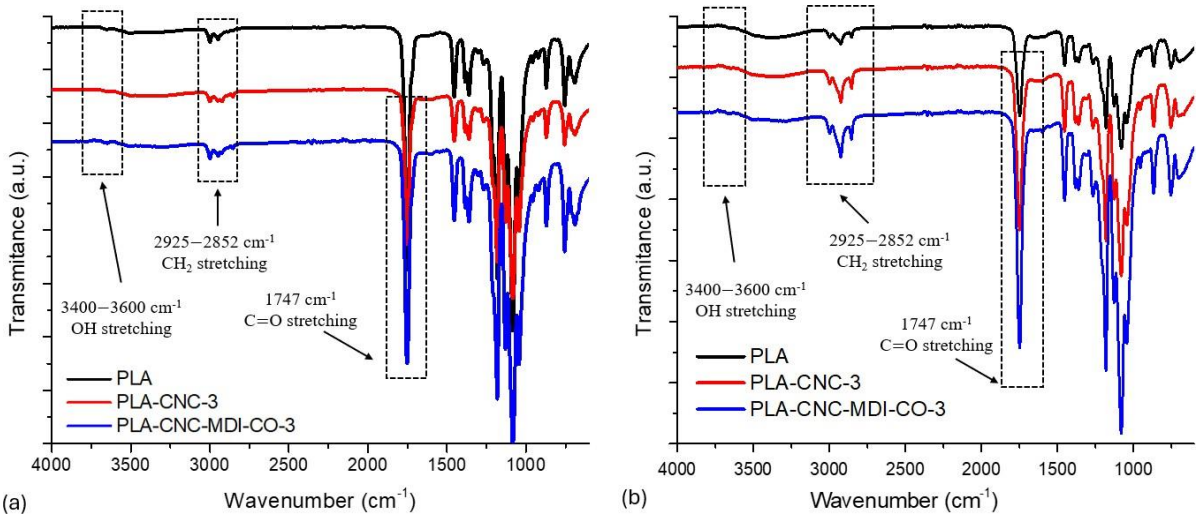



**Figure 4.14.** FTIR spectra of neat PLA and modified PLA composites that have been produced through (**a**) solvent casting (SC) and (**b**) Pickering emulsion (PE).

FTIR analysis reflects the molecular interactions and additive dispersion in PLA, PLA-CNC, and PLA-CNC-MDI-CO samples prepared by SC and PE methods. The appearance of some key peaks, such as C=O stretching (~1700 $cm^{-1}$) and C-O-C stretching (1000–1200 $cm^{-1}$), is more pronounced after the addition of CNC and the functionalization with MDI-castor oil, due to the successful integration of additives. In PE samples, much sharper and better-defined peaks may suggest a better molecular organization, superior dispersion, and stronger interfacial interactions than in SC samples with broader peaks, indicative of a more nonhomogeneous distribution. The PE method shows the highest percentage of chemical interactions and, hence, composite homogeneity compared to SC in these results.

## 4.8.8. DSC Analysis of CNC-PLA Nanocomposites

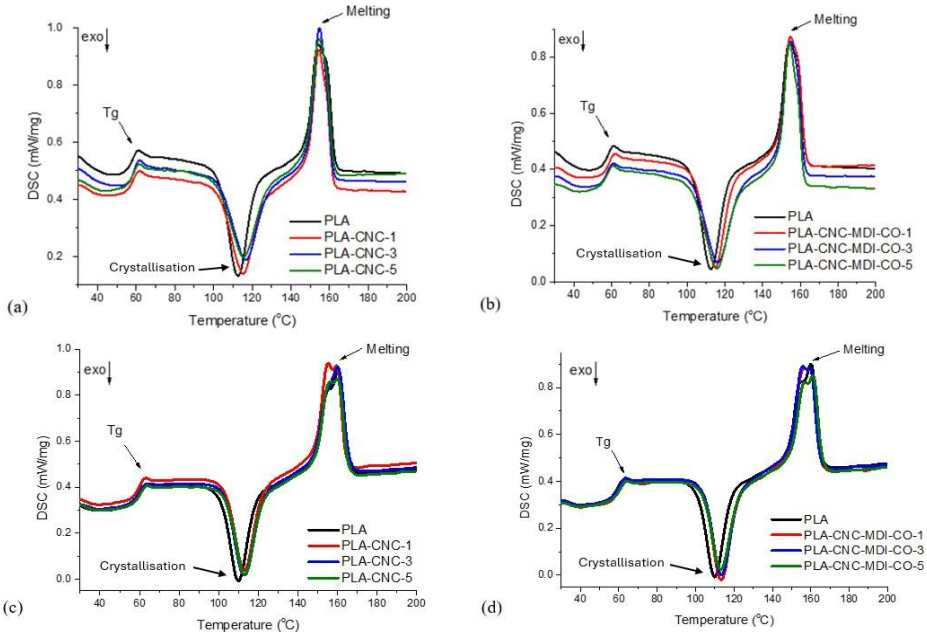



**Figure 4.15.** DSC profiles of (**a**) PLA-unmodified CNC samples (SC), (**b**) PLA-modified CNC samples (SC), (**c**) PLA-unmodified CNC samples (PE), and(**d**) PLA-modified CNC samples (PE).

**Table 5.** Thermal parameters of samples for solvent-casting (SC) and Pickering emulsion (PE) methods.

| Sample | $\Delta H_{cc}$ (J/g) | | $T_{cc}$ (°C) | | $\Delta H_m$ (J/g) | | $T_m$ (°C) | | $T_g$ (°C) | | $\chi$ (%) | |
|---|---|---|---|---|---|---|---|---|---|---|---|---|
| | SC | PE | SC | PE | SC | PE | SC | PE | SC | PE | SC | PE |
| PLA | 32.1 | 29.05 | 112.8 | 110.0 | 29.9 | 34.23 | 154.0 | 160.1 | 57.8 | 57.2 | 32.2 | 36.8 |
| PLA-CNC-1 | 33.1 | 30.15 | 115.3 | 113.1 | 26.7 | 34.44 | 154.5 | 159.5 | 58.5 | 58.1 | 28.7 | 37.0 |
| PLA-CNC-3 | 29.9 | 30.78 | 116.3 | 113.0 | 28.1 | 36.54 | 154.7 | 160.1 | 58.2 | 58.4 | 30.2 | 39.3 |
| PLA-CNC-5 | 30.8 | 28.27 | 115.5 | 113.3 | 28.6 | 33.29 | 154.5 | 160.0 | 58.3 | 58.9 | 30.8 | 35.8 |
| PLA-CNC-MDI-CO-1 | 30.8 | 29.40 | 115.1 | 113.4 | 29.3 | 35.27 | 154.6 | 159.5 | 58.6 | 57.6 | 31.5 | 37.9 |
| PLA-CNC-MDI-CO-3 | 30.9 | 32.09 | 116.2 | 113.6 | 28.4 | 34.53 | 154.8 | 159.4 | 57.2 | 57.9 | 30.5 | 37.1 |
| PLA-CNC-MDI-CO-5 | 30.6 | 29.77 | 115.8 | 113.3 | 27.8 | 32.58 | 154.4 | 161.1 | 57.6 | 58.2 | 29.9 | 35.0 |

The results of the DSC analysis of PLA-CNC nanocomposites prepared through solvent-casting and Pickering emulsion methods revealed key thermal characteristics. They demonstrated similar glass transition temperatures; however, the Pickering emulsion method improved crystallinity and thermal properties substantially. Accordingly, samples with the PE method could give better crystallization since nanoparticles had been acting as nucleation sites and could develop ordered structures that give rise to high melting enthalpy, ΔHm, with more thermal stability. By contrast, the SC samples showed lower crystallinity with wider cold crystallization enthalpy (ΔHcc) and a higher temperature of cold crystallization (Tcc), which points to more amorphous regions. The enhancement of crystallization and improvement in thermal properties for the PE method is due to the improved dispersion of particles and increased nucleation while plasticizing provided by castor oil played its part in the thermal response as well. The Tg was the same for the two methods.

## 4.8.9. TG Analysis of CNC-PLA Nanocomposites

**Table 6.** Percentage decomposition of neat PLA and PLA-CNC composites through solvent casting and Pickering emulsion.

| Sample | $T_{d5\%}$ (°C) | | $T_{d10\%}$ (°C) | | $T_{max}$ (°C) from DTG | | (%) Mass Loss | |
|---|---|---|---|---|---|---|---|---|
| | **SC** | **PE** | **SC** | **PE** | **SC** | **PE** | **SC** | **PE** |
| PLA | 124 | 331.3 | 304 | 341.8 | 367 | 367.4 | 99.95 | 99.82 |
| PLA-CNC-1 | 122 | 293.5 | 275 | 313.8 | 353 | 361.9 | 98.94 | 99.27 |
| PLA-CNC-3 | 120 | 301.6 | 277 | 321.4 | 345 | 361.8 | 98.56 | 99.98 |
| PLA-CNC-5 | 123 | 284.1 | 274 | 301.0 | 332 | 350.8 | 98.06 | 98.14 |
| PLA-CNC-MDI-CO-1 | 128 | 310.8 | 290 | 324.2 | 354 | 361.6 | 99.01 | 97.26 |
| PLA-CNC-MDI-CO-3 | 136 | 301.4 | 297 | 317.7 | 358 | 361.5 | 99.41 | 99.64 |
| PLA-CNC-MDI-CO-5 | 134 | 299.1 | 285 | 317.8 | 358 | 361.4 | 98.70 | 98.55 |

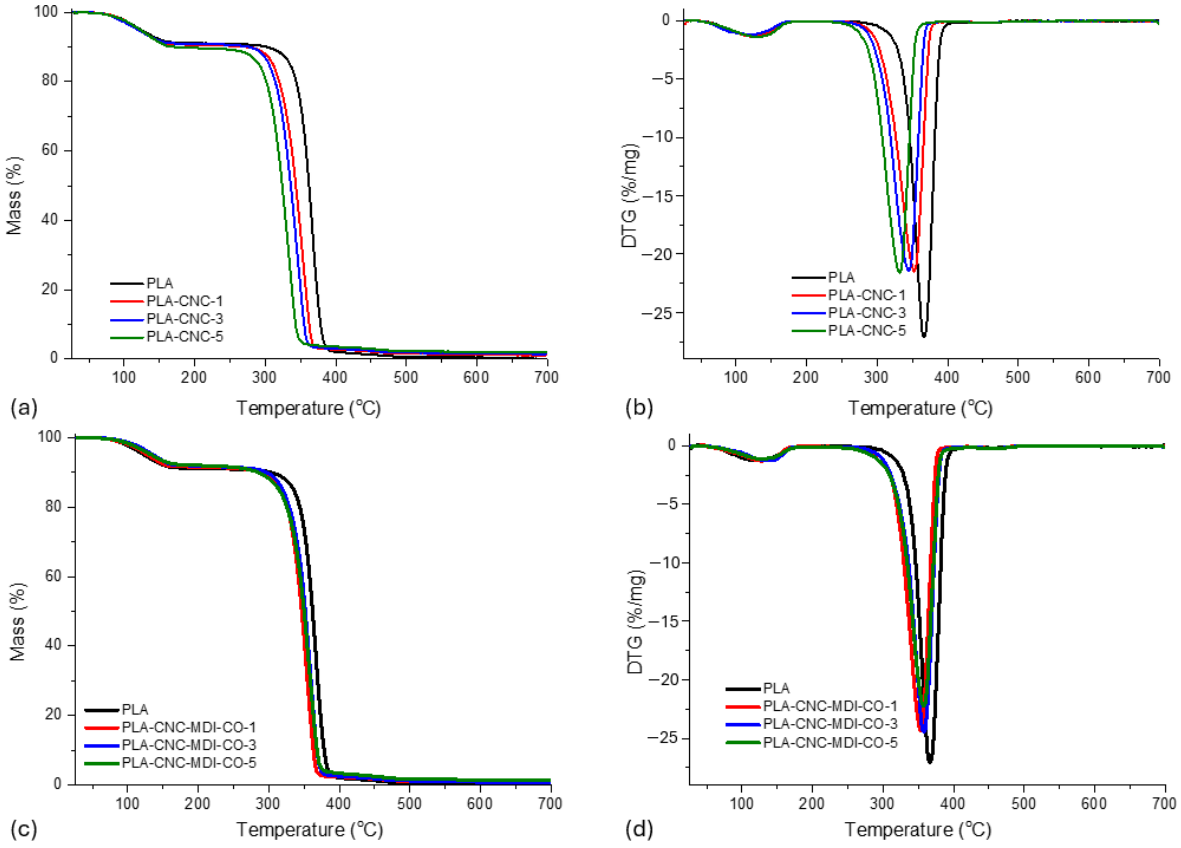



**Figure 4.16.** (**a**–**d**) Thermogravimetric analysis (TGA) and derivative thermogravimetric (DTG) curves for polylactic acid (PLA) and PLA composites produced via solvent casting.

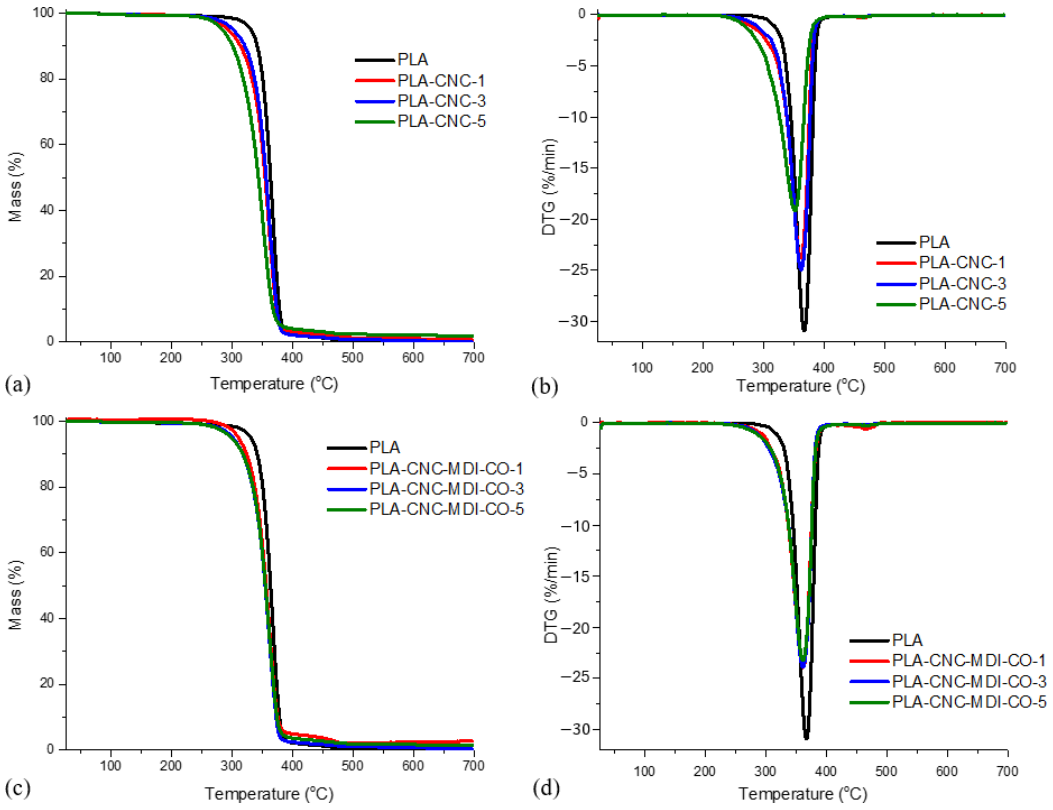



**Figure 4.17.** (**a**–**d**) Thermogravimetric analysis (TGA) and derivative thermogravimetric (DTG) curves for polylactic acid (PLA) and PLA composites produced via Pickering emulsion (PE).

TGA and DTG analyses of PLA-CNC and PLA-modified CNC samples produced by the solvent-casting method provide an overview of their thermal degradation behaviors. Neat PLA exhibits thermal degradation within the temperature range of 100–360°C, having a maximum degradation rate at 367°C. With the addition of CNC, slight reductions in the temperatures at which degradations take place were observed, while PLA-CNC-3 showed the lowest thermal stability. The addition of MDI and castor oil does change the degradation behavior; however, the overall trend is not significantly affected. The modified samples with similar or slightly lower mass loss than neat PLA reveal better thermal resistance in the PLA-CNC-MDI-CO samples.

Thermal properties of the composites by using Pickering emulsions: Neat PLA in this series of samples presents high thermal stability while undergoing degradation between 300-372°C. Generally, adding CNC reduces the thermal stability of the composite; however, the incorporation of MDI-CO improves thermal stability, which at 1% CNC is close to neat PLA. Higher CNC contents of 3% and 5% decrease the thermal stability; with the addition of MDI-CO, the properties improve. Generally, the method of Pickering emulsion is better than that of the solvent-casting method for thermal stability upon the addition of MDI-CO.

## 4.8.10. Mechanical Tests of PLA-CNC Nanocomposites

**Table 7.** Mechanical tests of solvent-casting and Pickering emulsion samples.

| Sample | Solvent Casting | | | Pickering Emulsion | | |
|---|---|---|---|---|---|---|
| | Young Modulus (MPa) | Tensile Strain (%) | Tensile Stress (MPa) | Young Modulus (MPa) | Tensile Strain (%) | Tensile Stress (MPa) |
| PLA | 1340.0 ± 21.6 | 23.5 ± 0.6 | 20.3 ± 0.3 | 2764.0 ± 53.2 | 3.97 ± 0.65 | 49.7 ± 1.2 |
| PLA-CNC-1 | 1034.6 ± 30.7 | 17.6 ± 0.5 | 20.1 ± 0.5 | 2825.2 ± 78.0 | 1.45 ± 0.12 | 35.2 ±3.8 |
| PLA-CNC-3 | 860.0 ± 27.7 | 11.0 ± 0.6 | 18.6 ± 0.5 | 2710.8 ± 87.5 | 1.12 ± 0.10 | 27.0 ± 2.2 |
| PLA-CNC-5 | 906.7 ± 46.8 | 9.8 ± 0.6 | 18.4 ± 0.5 | 2635.6 ± 76.9 | 0.82 ± 0.14 | 20.8 ± 3.8 |
| PLA-CNC-MDI-CO-1 | 1082.7 ± 20.6 | 8.4 ± 0.5 | 20.6 ± 0.3 | 2325.6 ± 29.3 | 1.87± 0.14 | 30.8 ± 1.2 |
| PLA-CNC-MDI-CO-3 | 1260.0 ± 20.5 | 5.0 ± 0.4 | 18.1 ± 0.3 | 2452.0 ± 59.6 | 1.05 ± 0.16 | 23.7 ± 3.3 |
| PLA-CNC-MDI-CO-5 | 1062.7 ± 18.3 | 5.3 ± 0.3 | 13.5 ± 0.2 | 2338.0 ± 79.9 | 0.78 ± 0.13 | 17.6 ± 3.1 |

The analysis focuses on the mechanical properties of neat PLA and its composites with cellulose nanocrystals and modified CNC, which are produced by solvent-casting and Pickering emulsion techniques at different concentrations. It can be observed from the results that the tensile strain of PLA composites generally decreases with an increase in CNC content. After the addition of CNC or modified CNC, it goes down from 20.3 MPa to 13.5 MPa for SC, and from 49.7 MPa to 17.7 MPa for PE method. With the addition of CNC, though stiffness improves, flexibility and tensile strength are reduced because of its rigid network structure. In the case of the solvent-casting method, a moderate increase in stiffness, for example, is recorded in PLA-CNC-3 with 860.0 MPa, but flexibility will be drastically reduced compared to pure PLA. Similarly, the increase in stiffness in the Pickering emulsion method continues only up to a certain CNC content and then decreases beyond that.

Addition of MDI and castor oil restores the flexibility and tensile strength to some extent. This has also improved the stiffness in solvent-cast samples, although it was still lower compared with that of pure PLA. Poor dispersion of CNC, MDI, and CO may result in weak interfacial bonding, which decreases the mechanical properties of the composites. PLA-CNC-MDI-CO-1 offers an optimal combination of stiffness, tensile strength, and strain, making it well-suited for semi-rigid or flexible packaging. Its balance of flexibility, moderate strength, and cost-effectiveness makes it an excellent choice for applications such as food wraps and medium-duty cartons. Comparing the two synthesis methods, the Pickering emulsion technique shows better results because of the improved dispersion and interaction between the PLA matrix and the additives. Overall, the results indicate that the addition of MDI and CO to CNC composites enhances their properties in flexible and semi-rigid packaging, offering a greener and more economical alternative to pure PLA.

4.8.11. Contact Angle (CA) Analysis of PLA-CNC Nanocomposites

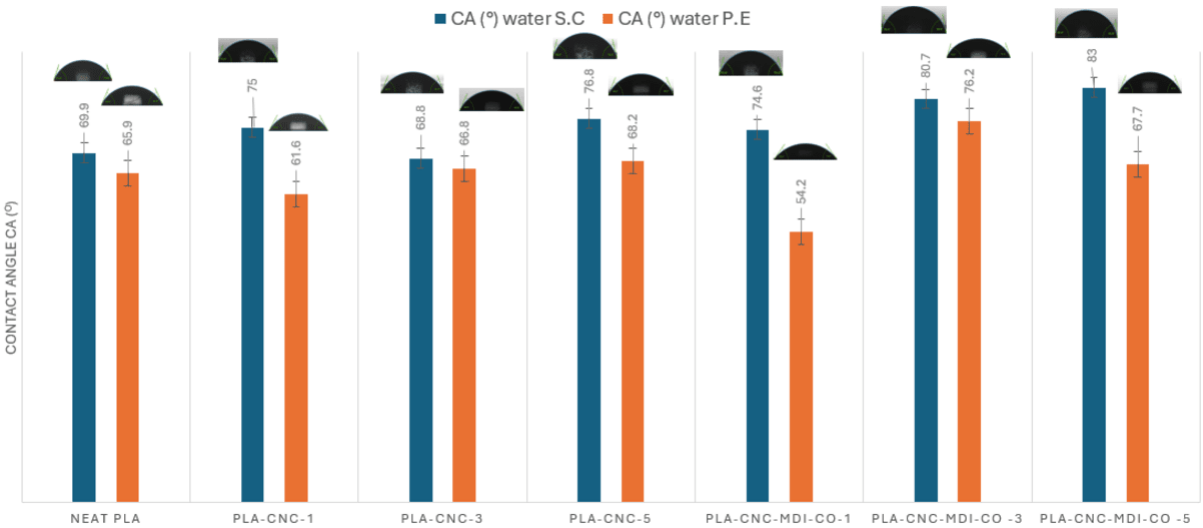



**Figure 4.18.** Water contact angle of neat PLA, and PLA composites through solvent-casting and Pickering emulsion methods.

This study presents the hydrophobicity and wettability of PLA-based composites with CNC, modified CNC, MDI, and castor oil. Improvement in hydrophobicity improves water resistance and thus enhances mechanical strength in a package. Neat PLA had a relatively lower contact angle of 69.9°, while CNC and modified CNC increased hydrophobicity. The addition of castor oil enhanced this further since castor oil itself has a hydrophobic nature; the contact angles were significantly increased.

The Pickering emulsion method yields more hydrophilic surfaces at low CNC concentrations but produces hydrophobic surfaces at higher concentrations of MDI and castor oil. The solvent-casting method generally yields more hydrophobic surfaces, especially with higher CNC and MDI/castor oil concentrations. The different surface structures obtained from each method influence the wettability of the composites.

## 4.8.12. SEM Analysis of PLA-CNC Nanocomposites

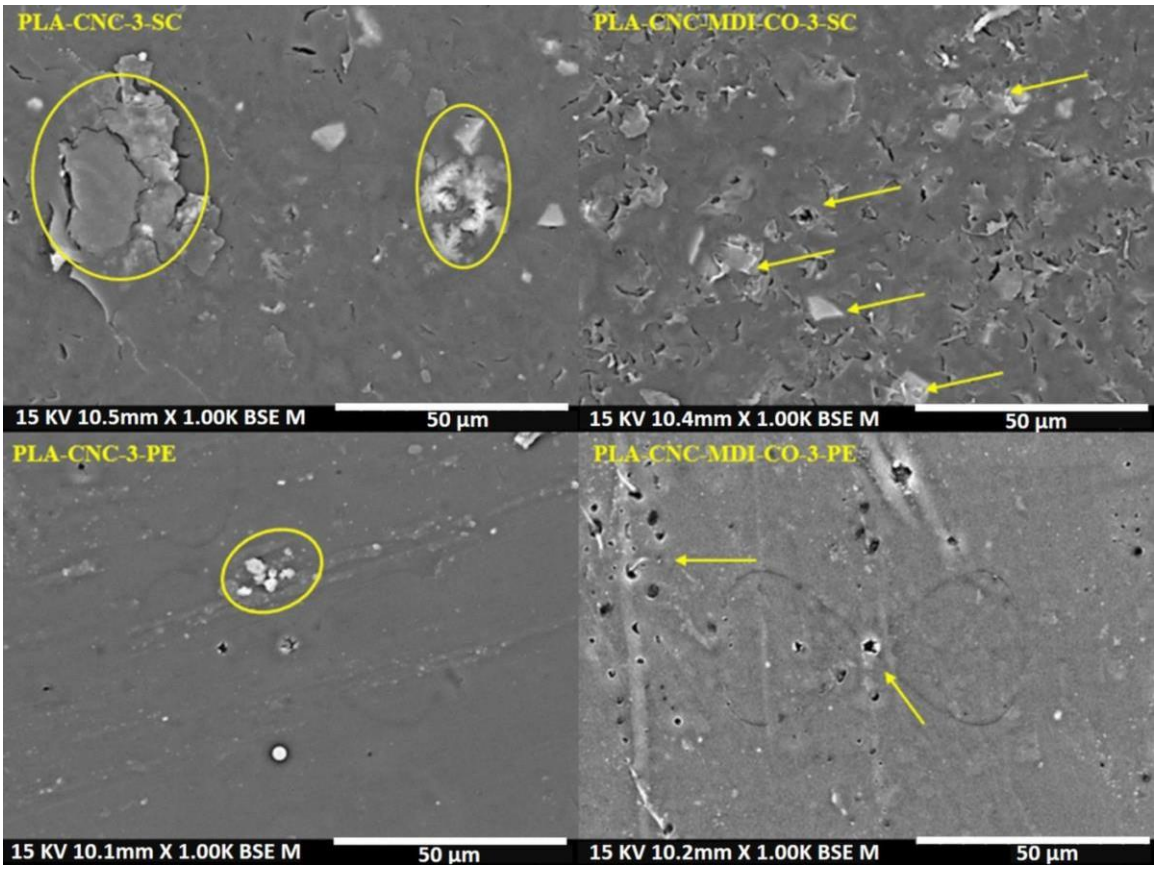



**Figure 4.19.** SEM images of PLA-CNC and PLA-modified CNC samples, which were prepared using solvent-casting (SC) and Pickering emulsion (PE) methods, with a concentration of 3% by mass.

The morphology of the PLA composites was characterized by SEM. Accordingly, considerable differences in the surface morphologies between PLA-CNC and PLA-modified CNC samples (with a content of 3% by mass) could be distinguished depending on the different ways of preparation. The SC method, PLA-CNC-3-SC, had a coarse surface appearance with visible agglomerates, which showed that the cellulose nanocrystal was not well dispersed and was highly clustered. In contrast, the PLA-CNC-3-PE prepared with the Pickering emulsion method had a smoother surface, indicating the more homogenous distribution of nanocrystals. This could be the reason for improved barrier performance and mechanical strength.

The surface of the PLA-CNC-MDI-CO-3-SC sample, prepared by the solvent-casting method, was more heterogeneous, with irregular features showing the complex microstructure that the addition of isocyanate and castor oil yields. On the other hand, the PLA-CNC-MDI-CO-3-PE sample, prepared by the Pickering emulsion method, had a smoother surface with some irregular features from the added components. These observations confirm that the preparation method and additives are very influential on the microstructure and properties of PLA composites.

## 4.9. Conclusions

This study focused on the modification of CNC with MDI and castor oil, improving its compatibility and interfacial adhesion, as revealed by FTIR and XPS analyses. However, the aggregation of CNC during its preparation and drying resulted in the formation of large microparticles instead of nanoparticles, which negatively affected the mechanical properties, especially for samples prepared by the solvent-casting method. The contact angle tests showed less hydrophobicity with the addition of castor oil, while thermal analysis showed good stability. SEM studies showed that the porosity and surface roughness increased, enhancing the flexibility and mechanical performance.

The second part of the work compared two preparation methods: solvent casting (SC) and Pickering emulsion (PE). The PE method gave better dispersion of CNC in the PLA matrix, as supported by FTIR and SEM results. The PE-based samples showed improved crystallinity, enhanced thermal stability, and a 15% increase in crystallinity, with better thermal stability—degrading at 335°C compared to 320°C for SC-based samples. PLA-CNC-MDI-CO-1 from the PE method achieved a balance of rigidity, ductility, and tensile strength, making it ideal for applications requiring moderate flexibility and strength. PE-based samples also presented enhanced hydrophobicity through improved dispersion. The results obtained in the current study indicated that the PE method is a more efficient approach to improving the molecular, thermal, and mechanical properties of CNC-PLA composites for sustainable biodegradable packaging material. Future studies will focus on the optimization of CNC, MDI, and castor oil concentrations and the improvement of the CNC aggregation problems to achieve better dispersion and performance.

# GENERAL CONCLUSIONS

This dissertation addresses the extraction, surface functionalization, and integration of cellulose nanomaterials (CNCs and CNFs) to enhance the properties of biodegradable polylactic acid composites, particularly for sustainable packaging. High-quality nanocellulose was successfully extracted from cotton fibers through both acid hydrolysis and enzymatic hydrolysis, with the latter offering a more environmentally friendly option. Surface modifications involving grafting with acrylic acid and furfuryl amine through Diels-Alder and Michael addition reactions result in a product with enhanced hydrophobicity and improved dispersibility in organic solvents. Furthermore, modified CNCs with castor oil-MDI significantly enhanced the mechanical and barrier properties of PLA composites.

The study compared two preparation methods, solvent casting (SC) and Pickering emulsion (PE), finding that the PE method provided better dispersion and reduced CNC agglomeration in the PLA matrix. The PE-based composites exhibited enhanced tensile strength, crystallinity, and thermal stability compared to the SC-based samples. Notably, the PE method resulted in a 15% increase in crystallinity, improving the mechanical properties and making the composites more suitable for scalable sustainable packaging applications. The incorporation of modified CNCs also significantly improved the hydrophobicity and overall properties of PLA composites, making them ideal candidates for packaging applications.

Future research should focus on optimizing environmentally friendly extraction methods, improving CNC dispersion, and further developing surface modification techniques to expand the use of these materials beyond packaging, such as in biomedicine and energy storage. Overall, this study demonstrates the potential of nanocellulose as a sustainable material and provides a foundation for future advancements in biodegradable composite technologies.

## SELECTIVE REFERENCES


**C-1/4.** Moon, R.J., Martini, A., Nairn, J., Simonsen, J., Youngblood, J. 2011. Cellulose nanomaterials review: structure, properties, and nanocomposites. Chem. Soc. Rev. 40, 3941.

**C-1/9.** M. Badiei, N. Asim, J. M. Jahim, and K. Sopian, "Comparison of chemical pretreatment methods for cellulosic biomass," APCBEE Procedia, vol. 9, pp. 170–174, 2014.

**C-1/13**. Ni, Y., & He, Z. Review: using magnesium hydroxide as the alkali source for peroxide bleaching of mechanical pulps-process chemistry and industrial implementation. Nordic Pulp & Paper Research Journal, vol. 25, no. 2, pp. 170–177, 2010.

**C-3/10**. Beltramino, F.; Roncero, M.B.; Vidal, T.; Torres, A.L.; Valls, C. Increasing yield of nanocrystalline cellulose preparation process by a cellulase pretreatment. *Bioresour. Technol.* **2015**, *192*, 574–581. [Google Scholar] [CrossRef]

**C-3/11**. Han, X.; Wang, J.; Wang, J.; Ding, L.; Zhang, K.; Han, J.; Jiang, S. Micro- and nano-fibrils of manau rattan and solvent-exchange-induced high-haze transparent holocellulose nanofibril film. *Carbohydr. Polym.* **2022**, *298*, 120075. [Google Scholar] [CrossRef]

**C-3/14**. Pandi, N.; Sonawane, S.H.; Kishore, K.A. Synthesis of cellulose nanocrystals (CNCs) from cotton using ultrasound-assisted acid hydrolysis. *Ultrason. Sonochem.* **2021**, *70*, 105353. [Google Scholar] [CrossRef]

**C-3/15**. Thambiraj, S.; Shankaran, D.R. Preparation and physicochemical characterization of cellulose nanocrystals from industrial waste cotton. *Appl. Surf. Sci.* **2017**, *412*, 405–416. [Google Scholar] [CrossRef]

**C-4/36**. Gonzalez Ortiz, D.; Pochat-Bohatier, C.; Cambedouzou, J.; Bechelany, M.; Miele, P. Current Trends in Pickering Emulsions: Particle Morphology and Applications. *Engineering* **2020**, *6*, 468–482. https://doi.org/10.1016/j.eng.2019.08.017.

**C-4/53**. Zhang, Y.; Cui, L.; Xu, H.; Feng, X.; Wang, B.; Pukánszky, B.; Mao, Z.; Sui, X. Poly(lactic acid)/cellulose nanocrystal composites via the Pickering emulsion approach: Rheological, thermal and mechanical properties. *Int. J. Biol. Macromol.* **2019**, *137*, 197–204. https://doi.org/10.1016/j.ijbiomac.2019.06.204.

**C-4/74**. de Carvalho-Guimarães, F.B.; Correa, K.L.; de Souza, T.P.; Rodríguez Amado, J.R.; Ribeiro-Costa, R.M.; Silva-Júnior, J.O.C. A Review of Pickering Emulsions: Perspectives and Applications. *Pharmaceuticals* **2022**, *15*, 1413. https://doi.org/10.3390/ph15111413.

## Scientific Publications

**Articles in Scientific Journals**

**Paper I**

A Comparative Study of the Impact of the Bleaching Method on the Production and Characterization of Cotton-Origin Nanocrystalline Cellulose by Acid and Enzymatic Hydrolysis

Polymers 2023, 15(16), 3446; https://doi.org/10.3390/polym15163446

Submission received: 30 June 2023 / Revised: 11 August 2023 / Accepted: 13 August 2023 / Published: 18 August 2023

**Paper II**

Nanocrystalline Cellulose Modification with Acrylic Acid and Furfuryl Amine Through Diels-Alder and Michael Addition Reactions.

U.P.B. Sci. Bull., Series B, Vol. 86, Iss. 2, 2024. ISSN 1454-2331

**Paper III**

Comparative Analysis of Solvent Casting and Pickering Emulsion Techniques for Improving the Mechanical Properties of Surface-Modified Cellulose Nanomaterial-Reinforced Polylactic Acid Composites

Polymers 2024, 16(23), 3406; https://doi.org/10.3390/polym16233406

Submission received: 4 November 2024 / Revised: 23 November 2024 / Accepted: 26 November

2024 / Published: 3 December 2024